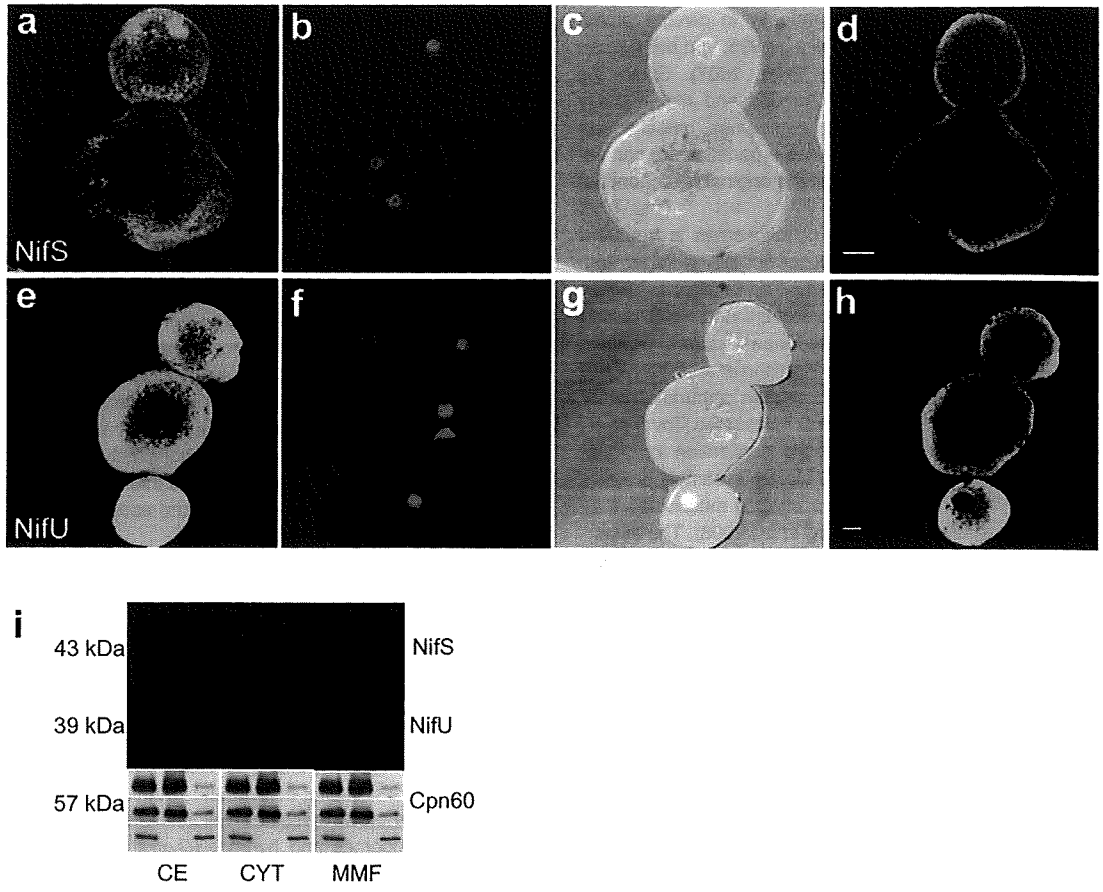

Fig. 1. Immunolocalization of *E. histolytica* Nif proteins by confocal microscopy and Western blotting. Fixed trophozoites were incubated with antibodies against EhNifS (A and D) or EhNifU (E and H) and post-treated with propidium iodide to identify nuclei (B and F). Panels A and E show maximum projections of stacked optical slices 1 m in thickness for NifS and NifU respectively. Corresponding single optical slices are shown on D and H; note that little or no antigen staining is apparent in the nucleus (compare bottom cell on E and H). Panels C and G show antibody and propidium iodide staining superimposed on DIC images.
I. Parasite cell-free extracts were fractionated by differential centrifugation and analysed by Western blotting; the specificity of antibodies used and the molecular mass of identified proteins are indicated. CE, crude extract; CYT, cytosolic fraction; MMF, mixed membrane fraction. Scale bars: 5 m.

transgenic *E. histolytica* lines ectopically expressing epitope-tagged variants of NifS and NifU either individually or simultaneously. Western blot analysis of transgenic parasite extracts demonstrated a 1.6-fold and a 2.6-fold overexpression of recombinant NifS and NifU respectively (Fig. S1). Confocal microscopy imaging confirmed that the overexpressed tagged variants colocalize with endogenous Nif proteins in transgenic trophozoites (data not shown but submitted for review), clearly indicating that the presence of epitope tags does not affect protein localization. Biochemical assays revealed a 1.5- and 2-fold enhancement of catalytic activity for the amoebal Fe-S proteins pyruvate : ferredoxin oxidoreductase and ferredoxin (Fig. 3) suggesting a direct correlation between Nif protein levels and Fe-S protein maturation. Interestingly, these transgenic parasite lines also displayed a growth phenotype suggesting that the activity of Fe-S proteins and the level of Nif protein expression can be growth rate limiting (Fig. S2).

Peroxide detoxification in mitosomes

The discovery that Nif proteins accumulate in *Entamoeba* mitosomes and the previous demonstration that NifS and NifU are necessary and sufficient for Fe-S cluster assembly suggested the existence of at least one Fe-S protein in

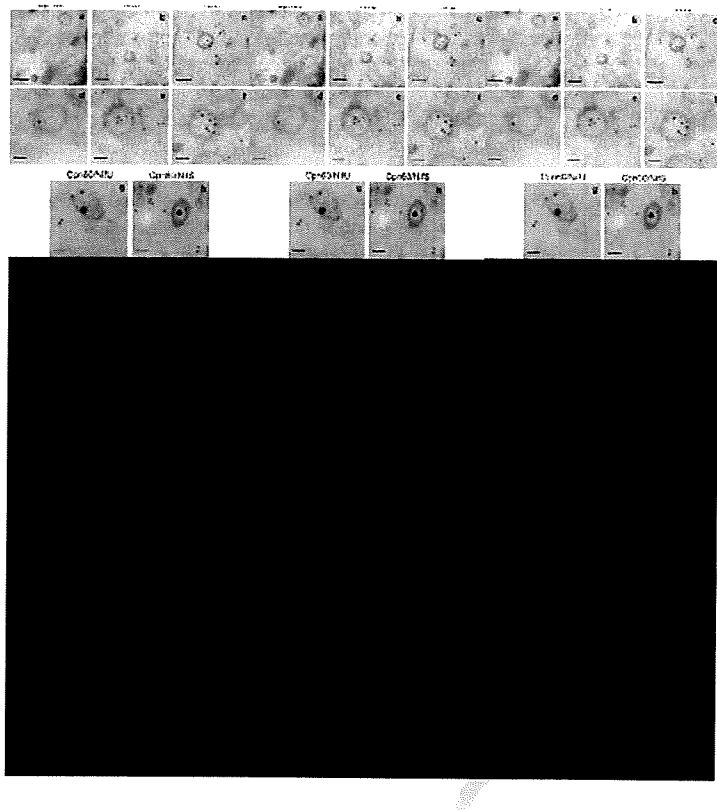

Fig. 2. Localization of amoebal NifS and NifU proteins by immunoelectron microscopy. Parasite trophozoites were fixed and embedded in resin as described in *Experimental procedures*. Ultra-thin sections were cut and mounted on grids before exposure to antibodies specific for EhCpn60 (A and D), EhNifU (B and E) or EhNifS (C and F). Double labelling using 20 nm gold particles for Cpn60 and 10 nm particles for Nif proteins is shown in G and H. Arrow heads highlight organellar membranes. Scale bars: 100 nm (A–C), 50 nm (D–F,G,H).

mitosomes that might require *in organello* maturation. Although none of the few known mitosomal proteins carries reactive Fe-S centres (Bakatselou *et al.*, 2000; 2003; León-Avila and Tovar, 2004; Chan *et al.*, 2005; van der Giezen *et al.*, 2005b; Aguilera *et al.*, 2008), the identification in the *Entamoeba* genome of a gene encoding rubrerythrin (Rbr) – a hydroperoxide detoxification Fe-S protein found predominantly in anaerobic bacteria but also recently discovered in *Trichomonas vaginalis* hydrogenosomes (Loftus *et al.*, 2005; Putz *et al.*, 2005) – suggested Rbr as a putative mitosomal protein in *E. histolytica*.

Bacterial Rbr contains an Fe $(S\text{-}Cys)_4$ reactive centre and a non-sulfur oxo-bridged diiron centre that are essential for functionality. All the cysteine, glutamate and histidine amino acid residues that form and hold these functional centres together are conserved in the amoebal Rbr homologue suggesting a functional amoebal peroxidase (Fig. 4A). We cloned and overexpressed this protein in a heterologous bacterial system. Affinity purified protein was then tested for functionality. NADPH-dependent peroxidase activity was observed when *E. histolytica* Rbr was added to an *in vitro* system containing NADPH, spinach ferredoxin : $NADP^+$ oxidoreductase, *Clostridium pasteurianum* rubredoxin (Rub) and H_2O_2 (Fig. 4B). This activity indicates that, analogous to prokaryotic Rbr and its *T. vaginalis* homologue, recombinant *E. histolytica* Rbr transfers electrons from Rub_{red} to peroxide, a process where electrons initially enter Rbr via the Fe $(SCys)_4$ centre and are then transferred to the diiron centre and on to peroxide (Coulter *et al.*, 1999). With a specific activity of 120 nmol min^{-1} mg^{-1} (corresponding to 3 mM min^{-1} mM^{-1}) recombinant *E. histolytica* Rbr was similar to that of recombinant *T. vaginalis* Rbr (125 nmol min^{-1} mg^{-1}). Specific activity of Rbr from the archaebacterium *Pyrococcus furiosus* and that of the proteobacterium *Desulfovibrio vulgaris* are three times and 20 times higher respectively (Coulter and Kurtz., 2001; Weinberg *et al.*, 2004). This difference may be due to the artificial electron-donor system in the *in vitro* assay, as Rub is the endogenous electron donor to Rbr in prokaryotes but is absent from the genomes of *E. histolytica* and *T. vaginalis*. In addition the His-tags at the C-termini of the recombinant eukaryotic proteins might interfere with dimerization, as the C-termini in active Rbr dimers lie at the subunit interface (Jin *et al.*, 2002).

Specific antibodies generated against recombinant *T. vaginalis* Rbr were then used in cell fractionation and

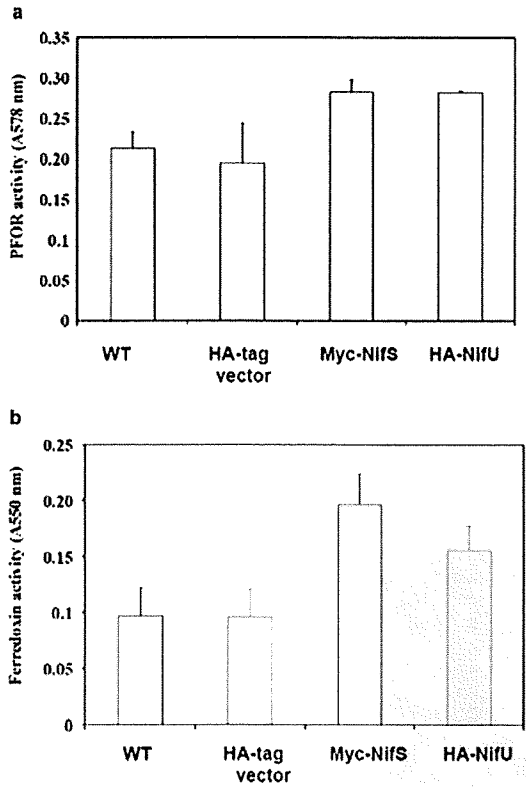

Fig. 3. Enhanced activity of FeS proteins in transgenic parasites by ectopic overexpression of amoebal NifS or NifU. Pyruvate: ferredoxin oxidoreductase (A) and ferredoxin (B) activities in *E. histolytica* trophozoites were measured in cell-free extracts as described in *Experimental procedures*. Bars represent the mean values and standard errors of data points collected in duplicate in at least two independent experiments. WT, untransfected parasites; HA-tag vector, control parasites transfected with the empty HA-tag expression vector; Myc-NifS, parasites overexpressing *myc*-tagged NifS protein; HA-NifU, parasites overexpressing HA-tagged NifU protein.

immunomicroscopy experiments to determine the intracellular distribution of amoebal Rbr. Confocal microscopy imaging demonstrated a punctuate distribution for this antigen in *Entamoeba* trophozites, revealing the presence of dozens of Rbr-containing compartments in every cell of the parasite population (Fig. 5A–E). Subcellular fractionation by differential centrifugation and separation of the MMF in sucrose density gradients identified a reactive antigen of the monomeric size predicted for *E. histolytica* Rbr in the high sucrose density fractions (Fig. 5F) further indicating the compartmentalization of Rbr in *Entamoeba*. Immunogold labelling of amoebal Rbr in ultra-thin transmission electron microscopy sections revealed the presence of highly abundant double membrane-bounded structures (Fig. 6A–D) of equivalent size and appearance to those observed with the anti-Cpn60 antibodies (Fig. 6E; see also Fig. 2). Double labelling for Rbr and Cpn60 localized both of these antigens in the same type of organelles demonstrating that *E. histolytica* Rbr is a mitosomal protein (Fig. 6F).

Redefinition of Entamoeba *mitosomes*

Considerable uncertainty had surrounded the ultrastructure of *E. histolytica* mitosomes (Aguilera *et al.*, 2008) as previous attempts to localize Cpn60 in electron microscopy micrographs proved unsuccessful (Ghosh *et al.*, 2000). Based on the immunoelectron microscopy data generated in our study it is now possible to define *E. histolytica* mitosomes as minute but abundant double membrane-bounded organelles housing the mitochondrial chaperonin Cpn60, Rbr and the Fe-S cluster assembly proteins NifS and NifU. At an estimated 100 nm in diameter and a mitosomal area of 7.9 10^{3} m^2, Nif labelling densities were 10-fold higher in mitosomes than in the cytosol demonstrating a significant enrichment of Fe-S cluster assembly proteins in these organelles (Table 1). Quantification in electron micrographs of labelled organelles allowed estimation of an average 34, 27, 37 and 29 mitosomes m^{3} for the NifS, NifU, Cpn60 and Rbr antigens respectively (see *Experimental proce-*

Table 1. Immunoelectron microscopy-based redefinition of *E. histolytica* mitosomes.

	Antigen			
Parameter	Cpn60	NifU	NifS	Rbr
Labelling density (golds m^{2})[a]				
Cytosol	2.3 ± 0.90	34 ± 5.2	32 ± 4.2	1.9 ± 1.1
Mitosomes	407 ± 38	357 ± 49	318 ± 29	306 ± 43
Mitosome : cytosol antigen distribution ratio	177	11	10	161
Mitosomes m^{3}	37	27	34	29
Mitosomes per trophozoite (10^{5})	1.54	1.13	1.42	1.21
Percentage of total cell volume	1.9	1.4	1.8	1.5

a. Labelling densities and organelle quantification were determined as described in *Experimental procedures* (n = 8 for Cpn60, n = 10 for NifU, n = 10 for NifS and n = 10 for Rbr; n = number of scanned micrographs).

a

```
E. histolytica      ---------------MATLINLCKAFAGESQARNRYLIYAKTAKKEGLDVIAQLFNETAN
T. vaginalis        ----------MSLKGTQTEKNLACAFAGESMARNRYTFFAEVAKKQGYEQIAQLFIETAE
M. jannashii        -----MINNFFVINMKETLKNLTKAYIGESLARNRYTCYAKIAKQEGYEQIAEIFLLTAE
A. fulgidus         ---------------MGTLENLVKAFIGESMARNRYTFYAKVAKDEGYVFIQRVFLETAE
P. gingivalis       MSIKKKTEMNKSIKGSKTEKHLLMAFAGESQARSRYTFFASVAKKEGYEQIAGVFMETAE
D. vulgaris         ---------MKALKGTKTERNILTAFAGESQARNRYDYFGARAKKDGFVQIADIFAETAS
                                          *  *** ** **       **  *   *   *  **
E. histolytica      QEGTHARILFEMIQSLKKE---GQETPKIE-TAVPIDFGTTADNLLAAIAGETYEHETMY
T. vaginalis        NEKVHANYFWSQIK---G-----LGSVKIETEVPACGVNDTLTNLRNAAAGEYAEHTTDY
M. jannashii        NEREHAKWLYYLITELKKKYNIDDKAIKVDGVEVPIVLGNTAENLKASIEGEHFEHTEMY
A. fulgidus         NEKEHAENLLKFIQQLRG----DNAAIKVE-AEAPLVWGTTVENLKAAIEGEHYENSEMY
P. gingivalis       QEKEHAKRFFSFLE---------GGMLEITASFPAGIIGSTAENLRAAAAGENEEWTDLY
D. vulgaris         QEKEHAKRLFKFLE---------GGEVEIVAAFPAGIIGDTHANLISSAAGENHEYTEMY
                     *  **                                  *  **    **  *    *
E. histolytica      PEFAKVAKEEGHAQIAARLNLIAKAELNHHNNYQKILDELKANSLYKKTEKVFWVCRECG
T. vaginalis        PHFADVAEKEGFAKIAKAFRGIAAVEKEHEIRFNTLAKQVESSTVFKREAVVAWKCRNCG
M. jannashii        PKFADIAEKEGLKEIADRLRAIGIAEKHHEERFKKLLKEVEEGTVFKKDKPVEWVCRKCG
A. fulgidus         PQFADEAEKEGFKDIADRLRAIGKAEEHHERRYRRLLAEVENGTFFKRDKEIAWVCLECG
P. gingivalis       PAFAETAEEEGFKEIAAVFRQIAKVEAEHERRYLALLAHVEDGSVFERTEEIAWQCRNCG
D. vulgaris         PSFARIAREEGFDEIAKVFMSIAVAEEFHERRFLGFAKNVKEARVFVRESSVVWRCRNCG
                    * **  *  **   **     *   *  *                          * *  **
E. histolytica      YIFESTQPPKVCPLCGEPGDFFRVQVSI--
T. vaginalis        YVVRAKVAPKACPVCFKPQGWFEIKEVLE-
M. jannashii        FVHLGKEPPEKCPSCSHPRKYFEVKCEKY-
A. fulgidus         YIHYGTEPPEECPSCGHPKAYYVAEDLLSL
P. gingivalis       YVITSKKAPKLCPACAHPQAYFEPMKTNY-
D. vulgaris         FLHEGNEAPHLCPACAHPQAHFELLGINW-
                           *  **  *  *
```

b

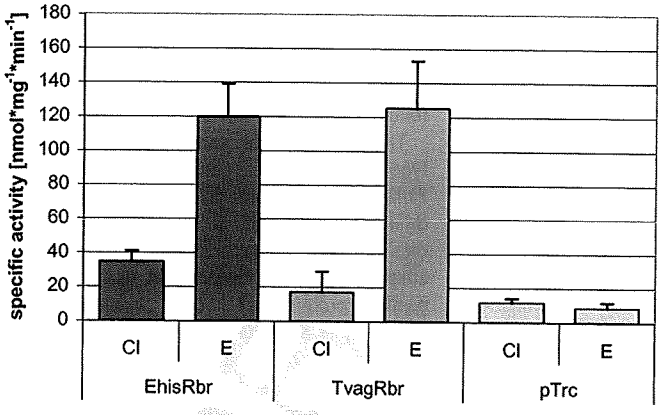

Fig. 4. Properties and functionality of *E. histolytica* rubrerythrin.
A. ClustalW alignment of eukaryotic rubrerythrin sequences with homologues from archaebacteria and eubacteria. Conserved glutamate and histidine residues holding the oxo-bridged diiron centre and cysteine residues involved in the Fe (S-Cys)$_4$ reactive centre (Coulter *et al.*, 1999) are shaded in grey.
B. Specific activity of recombinant His-tagged rubrerythrin from *E. histolytica* and *T. vaginalis*. pTrc, empty vector control; Cl, cleared lysate; E, Ni-NTA purified protein.

dures for calculations). Although *Entamoeba* trophozoites are pleomorphic, the size of an average amoeba is around 20 m in diameter (Müller, 2000) and its average cell volume is 4189 m^3. Thus an average trophozoite may contain over 100 000 mitosomes, a hitherto unsuspected abundance for these organelles in protozoan parasites (Table 1). Further, at an average mitosomal volume of 5.2 10^{-4} m^3 the total volume occupied by these organelles in *E. histolytica* may range between 60 and 82 m^3, representing approximately 1.4–1.9% of the total cell volume (Table 1). This figure represents only a fraction of the total cell volume occupied by other mitochondrial organelles (> 10% for mitochondria, 10% for trichomonad hydrogenosomes) (Müller, 2000) but it

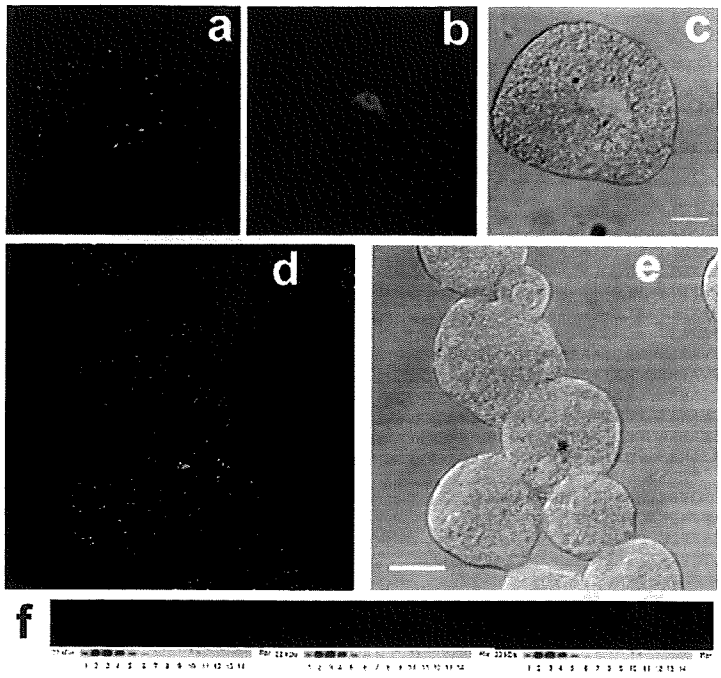

Colour

Fig. 5. Compartmentalized distribution of amoebal rubrerythrin.
A–E. Fixed parasite trophozoites were incubated with anti-TvRbr antibodies (A and D) and post-treated with propidium iodide to identify nuclei (B). (C and E) Superimposed DIC images showing individual cells. Scale bars: 5 m (C), 10 m (E).
F. *E. histolytica* cell-free extracts were separated by sucrose density gradient centrifugation as described in *Experimental procedures*. Fractions were then analysed by Western blotting using the anti-TvRbr antibodies. Fraction number (fractions collected from bottom of tube), antibody specificity and the molecular mass of identified protein bands are indicated.

compares favourably with the volume occupied by the amoebal nucleus (1.5%), suggesting that although mitosomes may no longer be involved in energy metabolism, they still likely represent important sites of metabolic flow in this parasite.

Discussion

Accumulating evidence indicates that mitochondria, mitosomes and hydrogenosomes are contemporary evolutionary endpoints of the original mitochondrial endosymbiont. In an extreme example of reductive organelle evolution *E. histolytica* has replaced its original mitochondrial Isc system of Fe-S cluster assembly with an analogous bacterial Nif system acquired by lateral gene transfer. The essential nature of compartmentalized Fe-S cluster assembly suggests that loss of the mitochondrial Isc system could only have taken place once the bacterial Nif system had been reliably adopted to function within *E. histolytica* mitosomes. That bacterial proteins other than those from the original mitochondrial endosymbiont were recruited during the course of evolution to function within mitochondria is reflected in the chimeric nature of the mitochondrial proteome (Kurland and Andersson, 2000; Esser *et al.*, 2004). The presence in *Entamoeba* mitosomes of bacterial-type Fe-S cluster assembly proteins takes this observation a step further and demonstrates that analogous protein replacement has also played an active role in the evolution of mitochondrion-related organelles.

The predominantly cytosolic distribution of bacterial-type Fe-S cluster assembly proteins NifS and NifU in *Entamoeba* contrasts with the predominantly mitochondrial localization of Fe-S cluster assembly in other eukaryotes (Lill and Mühlenhoff, 2008). In human cells a very small proportion of the cysteine desulfurase Nfu1 and the scaffold protein Isu1 – both essential for Fe-S cluster assembly – are found in cytosol and nuclei. However, maturation of both mitochondrial and extramitochondrial Fe-S proteins is known to require Fe-S clusters assembled in mitochondria. These are exported from the organelle via the Atm1/Erv1 export system (Gerber *et al.*, 2004; Lill and Mühlenhoff, 2008). In *Entamoeba*, Fe-S centres synthesized in the cytosol are unlikely to be available for the maturation of mitosomal Fe-S proteins. This would require a specific cytosol-to-mitosome Fe-S cluster import system equivalent to but of reverse flux to the Atm1/Erv1-mediated mitochondrial export system. That no homologues of such transport proteins have been found in the *E. histolytica* genome suggests that these vital cofactors are not transported through membranes in this organism (Loftus *et al.*, 2005; Clark *et al.*, 2007).

Instead, the recruitment of a significant proportion of the Fe-S cluster assembly proteins NifS and NifU into *Enta-*

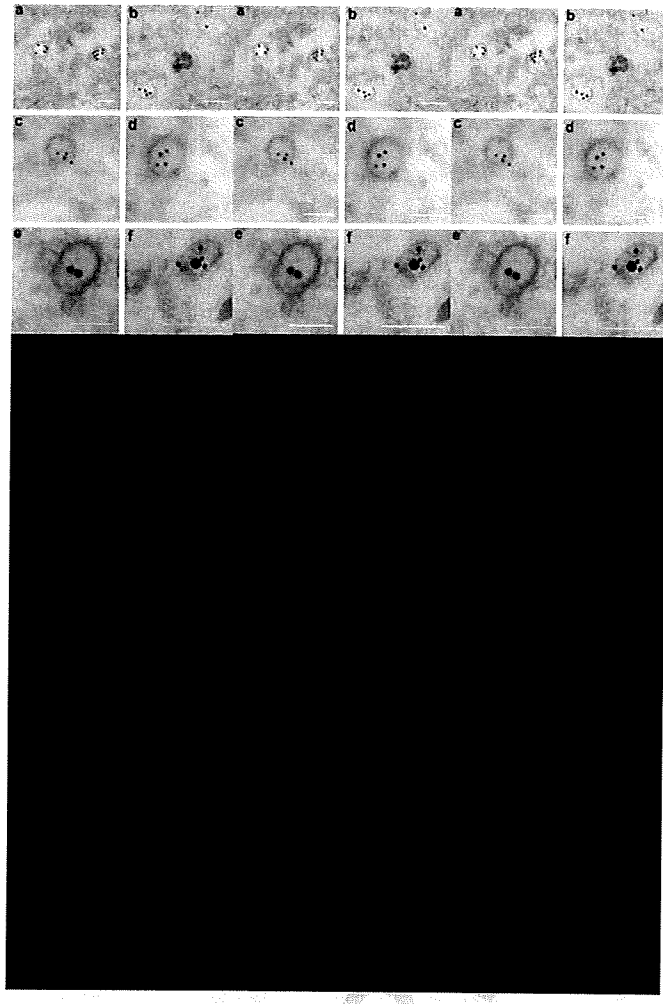

Fig. 6. Localization of *E. histolytica* rubrerythrin by immunoelectron microscopy. Fixed parasite trophozoites were embedded in resin and ultra-thin sections were mounted on grids before incubation with antibodies specific for TvRbr (A–D) or EhCpn60 (E). Double labelling using 20 nm gold particles for Cpn60 and 10 nm gold particles for Rbr is shown in F. Arrowheads in c indicate the organellar membranes. Scale bars: 100 nm.

moeba mitosomes – estimated at around 17% from the average cell volume occupied by mitosomes and from the 10-fold enrichment of Nif proteins in these organelles – suggests that compartmentalized Fe-S cluster biosynthesis in *E. histolytica* is required for the *in organello* maturation of mitosomal proteins. At present it is unclear how bacterial proteins such as NifS, NifU and Rbr are imported into mitosomes as they lack typical amino-terminal targeting peptides to aid their passage across mitosomal membranes. However, protein import into mitosomes has been shown to proceed via both presequence-dependent and -independent mechanisms (Tovar *et al.*, 1999; Dolezal *et al.*, 2005; Regoes *et al.*, 2005). Moreover, the natural predisposition of some bacterial proteins for mitochondrial targeting has been demonstrated (Lucattini *et al.*, 2004).

Despite multiple efforts and the availability of the *E. histolytica* genome sequence no biological function had been assigned to amoebal mitosomes, until now (Loftus *et al.*, 2005; Clark *et al.*, 2007; Aguilera *et al.*, 2008). For years it has been known that *E. histolytica* is capable of metabolizing oxygen with high affinity without the accumulation of peroxide (Reeves, 1984; Müller, 2003). In the absence of catalase and glutathione peroxidase it had been assumed that cytosolic peroxiredoxins and the thioredoxin/thioredoxin reductase system were responsible for the removal of hydroperoxides from the cell (Choi *et al.*, 2005; Davis *et al.*, 2006; Arias *et al.*, 2007). The identification of Rbr in mitosomes adds another dimension to the hydroperoxide detoxification capabilities of *E. histolytica.* Its functional Fe-S centres could allow Rbr to participate in

the transfer of electrons from organic donors to oxygen via reduction of hydrogen peroxide, thus preventing its accumulation and toxicity inside these organelles. Whether oxygen metabolism occurs primarily in mitosomes or in the cytoplasm remains to be determined experimentally but the Rbr-dependent removal of toxic hydrogen peroxide in mitosomes could help the parasite survive the fluctuating low oxygen concentrations within the human intestine and, most importantly, the high concentrations of oxygen it encounters in the portal system during invasive amoebiasis (Stanley, 2003).

It has recently been reported that Rbr is upregulated in *E. histolytica* trophozoites exposed to oxidative stress clearly supporting the role of this mitosomal enzyme in hydroperoxide detoxification (Vicente *et al.*, 2009). We conclude that Fe-S cluster biosynthesis and Fe-S protein-mediated oxygen detoxification are fundamental functions of *E. histolytica* mitosomes which together could have selected for the retention of the original mitochondrial endosymbiont in this microaerophilic eukaryote.

Experimental procedures

Cell culturing and subcellular fractionation

Entamoeba histolytica HM-1:IMSS parasites were cultured in YI-S medium supplemented with 15% adult bovine serum as described (Diamond *et al.*, 1995). Axenically grown trophozoites were harvested by centrifugation, washed twice in PBS, resuspended in PBS/PI/E64 [PBS containing Protease inhibitor cocktail (Roche) and 50 M E64 (Sigma)] and lysed by freeze-thawing. After an initial centrifugation for 10 min at 1000 *g* the post-nuclear supernatant was subjected to ultracentrifugation at 100 000 *g* for 1 h at 4°C to produce a high-speed supernatant (the cytosolic fraction) and a high-speed sediment (MMF) containing broken membranes and membrane-bounded organelles. The MMF was subsequently washed twice and resuspended in PBS/PI/E64. In some experiments both the post-nuclear supernatant and the MMF were further fractionated by density gradient centrifugation and fractions collected from the bottom of tubes. Samples were then subjected to Western blot analyses as described below. Protein concentrations were determined by the Bradford method (Bradford, 1976) using a commercial protein assay solution (Bio-Rad).

SDS-PAGE, sample preparation and Western blotting

Protein samples were mixed (1:1) with 2 Laemli sample buffer (Sigma) and heated at 96°C for 5 min prior to the SDS-PAGE. Ten microlitres of sample was loaded onto NuPAGE® 10% BIS-TRIS gels (Invitrogen) and separated at 150 V. For Western blotting, proteins were transferred onto a nitrocellulose membrane (Bio-Rad) at 150 V for 1 h. The membranes were blocked in 4% (w/v) skimmed milk in TBS-T buffer (Tris-buffer saline with 0.1% Tween 20) for 1 h at room temperature and subsequently incubated at 4°C overnight with primary antibodies (anti-TvRbr; 1:1000; anti-EhCpn60, anti-EhNifS, anti-EhNifU; all three 1:5000 in blocking solution). Following washing in TBS-T membranes were further incubated with secondary Immunopure® peroxidase-conjugated goat anti-rabbit antibody (Pierce; 1:20 000 in blocking solution) for 1 h at room temperature. Blots were developed using an ECL detection system (GE Healthcare).

Immunofluorescence confocal microscopy

Entamoeba trophozoites were fixed in 4% paraformaldehyde in PBS for 30 min at 37°C, washed in PBS and permeabilized with 0.2% triton X-100 in PBS. Cells were then attached to poly-L-lysine-coated microscopic slides and exposed to blocking solution (3% BSA in PBS) for 3 h at room temperature, before incubation with antigen-specific primary antibodies (diluted 1:200 in blocking solution) overnight at 4°C. Control slides were incubated with pre-immune serum and/or blocking solution. Following 4 washing in PBS containing 0.2% Triton X-100 slides were incubated with secondary Alexa Fluor ®488 goat anti-rabbit antibody (1:500 in blocking solution, Invitrogen) for 1 h at 37°C. Slides were further washed in PBS, mounted with 1:1 mixture of VectaShield and 0.4 g ml ^{1} propidium iodide and observed under a laser scanning confocal microscope (Radiance 2100, Bio-Rad). Z-stacks (optical slices 0.5 or 1 m in thickness) were collected using Bio-Rad LaserSharp 2000 software and further processed using Adobe Photoshop V7.0 and/or ImageJ (http://rsb.info.nih.gov/ij/) software packages. 3

Immunoelectron microscopy

Entamoeba trophozoites were fixed in 4% paraformaldehyde in PBS for 30 min at 37°C, washed in PBS and gradually dehydrated in ethanol (30–100%), infiltrated and embedded in K4M resin. Thin sections (70–100 nm thick) were cut with a diamond knife and mounted onto gold grids. Immunogold labeling was done on grids floating on drops. The samples were blocked and incubated with single primary antibodies (anti-EhCpn60, anti-TvRbr, anti-EhNifS or anti-EhNifU; all 1:50 and 1:200 dilutions – pre-immune serum or blocking solution were used in control grids) followed with secondary goat anti-rabbit IgG conjugated to immunogold particles of either 10 nm or 20 nm in diameter (BB International; 1:100 dilution in blocking buffer). Double labeling experiments were carried out in the same way but with an additional paraformaldehyde vapor treatment step between antibody incubations as previously described (Mahendrasingam *et al.*, 2003). Labeled samples were then post stained with uranyl acetate and lead citrate and observed under a Hitachi H-7600 transmission electron microscope. Digital images were collected and stored as TIFF files and further processed using Adobe Photoshop V7.0 and/or ImageJ (http://rsb.info.nih.gov/ij/) software packages. 4

Immunoelectron microscopy quantification and calculations

Labeling densities were estimated by counting the number of gold particles on electronic micrographs layered with square lattice grids of 20 and 100 nm in Adobe Photoshop. Labeling densities in cytosol represent the number of gold particles not associated with biological membranes per square micron on thin

sections. Organelle labeling densities were estimated by first determining the average number of gold particles per labeled organelle (total number of gold particles associated with membrane-bounded organelles per square micron divided by the total number of gold-labeled organelles in the same area) and then dividing the resulting values by the area of an organelle 100 nm in diameter (7.85 10^{3} m^2). In parallel calculations that take into account the thickness of the thin sections imaged (100 nm maximum) the average number of labeled organelles per square micron was multiplied by 100 to estimate the average number of organelles per cubic micron (m^3). Resulting values were then multiplied by the total volume of an average spherical trophozoite of 20 microns in diameter (4189 m^3) to estimate the average number of organelles per parasite trophozoite. Similarly, the volume occupied by an average spherical organelle of 100 nm in diameter (5.2 10^{4} m^3) was multiplied by the total number of organelles in a cell to determine the overall volume occupied by labeled organelles. These values were then divided by the average volume of a trophozoite and multiplying by 100 to express them as percentages of cell volume. Standard equations for calculating the area of a circle (r^2) and the volume of a sphere (4/3 r^3) were used as appropriate.

Enzymatic assays

Affinity purified, recombinant *E. histolytica* and *T. vaginalis* Rbr were tested for NADPH-dependent peroxidase activity in reaction mixtures containing 25 g Rbr, 100 M NADPH, 0.5 M ferredoxin : $NADP^+$ oxidoreductase from spinach, 0.5 M rubredoxin from *C. pasteurianum*, 250 M H_2O_2, 50 mM MOPS pH 7.0, 0.1 mM EDTA, 20 mM glucose, 0.1 U ml^{1} glucose oxidase (all enzymes purchased from Sigma). Assays were covered with butanol and extinction at 340 nm was followed in a Genesys 10 UV photometer at room temperature.

Ferredoxin and pyruvate: ferredoxin oxidoreductase activities were monitored in cell-free extracts following reduction of cytochrome *c* at 550 nm and of methyl viologen or nitroblue tetrazolium at 578 nm respectively. Extracts were prepared from 30 to 50 mg of cell pellets suspended in 200 l of 50 mM Tris-HCl buffer pH 9.0, 1 mM EDTA, 2.0 mM DTT, 15% glycerol supplemented with protease inhibitors (E64 and Complete Mini Cocktail, Roche), sonicated and centrifuged at 10 000 *g*. The supernatant was collected and used in enzymatic reactions.

Acknowledgements

We thank Neil Sommerville for parasite culture and Patricia Goggin (Southhampton University) for advice and help with the initial electron microscopy work. The participation of Dr Gloria León-Avila and Mr Adhiraj Chakrabarty in preliminary work related to this project is acknowledged. This work was supported by a project grant from the BBSRC (BB/C507145) to J.T.

References

Aguilera, P., Barry, T., and Tovar, J. (2008) *Entamoeba histolytica* mitosomes: organelles in search of a function. *Exp Parasitol* 118: 10–16.

Ali, V., Shigeta, Y., Tokumoto, U., Takahashi, Y., and Nozaki, T. (2004) An intestinal parasitic protist, *Entamoeba histolytica*, possesses a non-redundant nitrogen fixation-like system for iron-sulfur cluster assembly under anaerobic conditions. *J Biol Chem* 279: 16863–16874.

Arias, D.G., Gutierrez, C.E., Iglesias, A.A., and Guerrero, S.A. (2007) Thioredoxin-linked metabolism in *Entamoeba histolytica*. *Free Radic Biol Med* 42: 1496–1505.

Bakatselou, C., Kidgell, C., and Clark, C.G. (2000) A mitochondrial-type hsp70 gene of *Entamoeba histolytica*. *Mol Biochem Parasitol* 110: 177–182.

Bakatselou, C., Beste, D., Kadri, A.O., Somanath, S., and Clark, C.G. (2003) Analysis of genes of mitochondrial origin in the genus *Entamoeba*. *J Eukaryot Microbiol* 50: 210–214.

Beinert, H. (2000) Iron-sulfur proteins: ancient structures, still full of surprises. *J Biol Inorg Chem* 5: 2–15.

Beinert, H., Holm, R.H., and Munck, E. (1997) Iron-sulfur clusters: nature's modular, multipurpose structures. *Science* 277: 653–659.

Bradford, M.M. (1976) A rapid and sensitive method for the quantitation of microgram quantities of protein utilizing the principle of protein-dye binding. *Anal Biochem* 72: 248–254.

Chan, K.W., Slotboom, D.J., Cox, S., Embley, T.M., van der Fabre, O., G.M., et al. (2005) A novel ADP/ATP transporter in the mitosome of the microaerophilic human parasite *Entamoeba histolytica*. *Curr Biol* 15: 737–742.

Choi, M.H., Sajed, D., Poole, L., Hirata, K., Herdman, S., Torian, B.E., *et al.* (2005) An unusual surface peroxiredoxin protects invasive *Entamoeba histolytica* from oxidant attack. *Mol Biochem Parasitol* 143: 80–89.

Clark, C.G., Alsmark, U.C., Tazreiter, M., Saito-Nakano, Y., Ali, V., Marion, S., *et al.* (2007) Structure and content of the *Entamoeba histolytica* genome. *Adv Parasitol* 65: 51–190.

Coulter, E.D., and Kurtz, D.M., Jr (2001) A role for rubredoxin in oxidative stress protection in *Desulfovibrio vulgaris*: catalytic electron transfer to rubrerythrin and two-iron superoxide reductase. *Arch Biochem Biophys* 394: 76–86.

Coulter, E.D., Shenvi, N.V., and Kurtz, D.M., Jr (1999) NADH peroxidase activity of rubrerythrin. *Biochem Biophys Res Commun* 255: 317–323.

Craig, E.A., and Marszalek, J. (2002) A specialized mitochondrial molecular chaperone system: a role in formation of Fe/S centers. *Cell Mol Life Sci* 59: 1658–1665.

Davis, P.H., Zhang, X., Guo, J., Townsend, R.R., and Stanley, S.L., Jr (2006) Comparative proteomic analysis of two *Entamoeba histolytica* strains with different virulence phenotypes identifies peroxiredoxin as an important component of amoebic virulence. *Mol Microbiol* 61: 1523–1532.

Diamond, L.S., Clark, C.G., and Cunnick, C.C. (1995) YI-S, a casein-free medium for axenic cultivation of *Entamoeba histolytica*, related *Entamoeba, Giardia intestinalis and Trichomonas vaginalis*. *J Eukaryot Microbiol* 42: 277–278.

Dolezal, P., Smid, O., Rada, P., Zubacova, Z., Sutak, R., Nebesarova, J., *et al.* (2005) *Giardia* mitosomes and trichomonad hydrogenosomes share a common mode of protein targeting. *Proc Natl Acad Sci USA* 102: 10924–10929.

Embley, T.M. (2006) Multiple secondary origins of the

anaerobic lifestyle in eukaryotes. *Philos Trans R Soc Lond B Biol Sci* 361: 1055–1067.

Embley, T.M., Finlay, B.J., Dyal, P.L., Hirt, R.P., Wilkinson, M., and Williams, A.G. (1995) Multiple origins of anaerobic ciliates with hydrogenosomes within the radiation of aerobic ciliates. *Proc R Soc Lond B Biol Sci* 262: 87–93.

Embley, T.M., van der Giezen, M., Horner, D.S., Dyal, P.L., Bell, S., and Foster, P.G. (2003) Hydrogenosomes, mitochondria and early eukaryotic evolution. *IUBMB Life* 55: 387–395.

Esser, C., Ahmadinejad, N., Wiegand, C., Rotte, C., Sebastiani, F., Gelius-Dietrich, G., *et al.* (2004) A genome phylogeny for mitochondria among alpha-proteobacteria and a predominantly eubacterial ancestry of yeast nuclear genes. *Mol Biol Evol* 21: 1643–1660.

Frazzon, J., and Dean, D.R. (2003) Formation of iron-sulfur clusters in bacteria: an emerging field in bioinorganic chemistry. *Curr Opin Chem Biol* 7: 166–173.

Gerber, J., Neumann, K., Prohl, C., Mühlenhoff, U., and Lill, R. (2004) The yeast scaffold proteins Isu1p and Isu2p are required inside mitochondria for maturation of cytosolic Fe/S proteins. *Mol Cell Biol* 24: 4848–4857.

Ghosh, S., Field, J., Rogers, R., Hickman, M., and Samuelson, J. (2000) The *Entamoeba histolytica* mitochondrion-derived organelle (crypton) contains double-stranded DNA and appears to be bound by a double membrane. *Infect Immun* 68: 4319–4322.

van der Giezen, M., Cox, S., and Tovar, J. (2004) The iron-sulphur cluster assembly genes *iscS* and *iscU* of *Entamoeba histolytica* were acquired by horizontal gene transfer. *BMC Evol Biol* 4: 7.

van der Giezen, M., Tovar, J., and Clark, C.G. (2005a) Mitochondrion-derived organelles in protists and fungi. *Int Rev Cytol* 244: 177–227.

van der Giezen, M., León-Avila, G., and Tovar, J. (2005b) Characterization of chaperonin 10 (Cpn10) from the intestinal human pathogen *Entamoeba histolytica*. *Microbiology* 151: 3107–3115.

Gill, E.E., Diaz-Trivino, S., Barbera, M.J., Silberman, J.D., Stechmann, A., Gaston, D., *et al.* (2007) Novel mitochondrion-related organelles in the anaerobic amoeba *Mastigamoeba balamuthi*. *Mol Microbiol* 66: 1306–1320.

Goldberg, A.V., Molik, S., Tsaousis, A.D., Neumann, K., Kuhnke, G., Delbac, F., *et al.* (2008) Localization and functionality of microsporidian iron-sulphur cluster assembly proteins. *Nature* 452: 624–628.

Jin, S., Kurtz, D.M., Jr., Liu, Z.J., Rose, J., and Wang, B.C. (2002) X-ray crystal structures of reduced rubrerythrin and its azide adduct: a structure-based mechanism for a non-heme diiron peroxidase. *J Am Chem Soc* 124: 9845–9855.

Katinka, M.D., Duprat, S., Cornillot, E., Metenier, G., Thomarat, F., Prensier, G., *et al.* (2001) Genome sequence and gene compaction of the eukaryote parasite *Encephalitozoon cuniculi*. *Nature* 414: 450–453.

Kurland, C.G., and Andersson, S.G. (2000) Origin and evolution of the mitochondrial proteome. *Microbiol Mol Biol Rev* 64: 786–820.

León-Avila, G., and Tovar, J. (2004) Mitosomes of *Entamoeba histolytica* are abundant mitochondrion-related remnant organelles that lack a detectable organellar genome. *Microbiology* 150: 1245–1250.

Lill, R., and Kispal, G. (2000) Maturation of cellular Fe-S proteins: an essential function of mitochondria. *Trends Biochem Sci* 25: 352–356.

Lill, R., and Mühlenhoff, U. (2008) Maturation of iron-sulfur proteins in eukaryotes: mechanisms, connected processes, and diseases. *Annu Rev Biochem* 77: 1–32.

Loftus, B., Anderson, I., Davies, R., Alsmark, U.C., Samuelson, J., Amedeo, P., *et al.* (2005) The genome of the protist parasite *Entamoeba histolytica*. *Nature* 433: 865–868.

Loiseau, L., Ollagnier-d., e-Choudens, S., Nachin, L., Fontecave, M., and Barras, F. (2003) Biogenesis of Fe-S cluster by the bacterial Suf system: SufS and SufE form a new type of cysteine desulfurase. *J Biol Chem* 278: 38352–38359.

Lucattini, R., Likic, V.A., and Lithgow, T. (2004) Bacterial proteins predisposed for targeting to mitochondria. *Mol Biol Evol* 21: 652–658.

Mahendrasingam, S., Wallam, C.A., and Hackney, C.M. (2003) Two approaches to double post-embedding immunogold labeling of freeze-substituted tissue embedded in low temperature Lowicryl HM20 resin. *Brain Res Brain Res Protoc* 11: 134–141.

Morrison, H.G., McArthur, A.G., Gillin, F.D., Aley, S.B., Adam, R.D., Olsen, G.J., *et al.* (2007) Genomic minimalism in the early diverging intestinal parasite *Giardia lamblia*. *Science* 317: 1921–1926.

Müller, M. (2000) A mitochondrion in *Entamoeba histolytica*? *Parasitol Today* 16: 368–369.

Müller, M. (2003) Energy metabolism. Part I: anaerobic protozoa. In *Molecular Medical Parasitology*. Marr, J., Nilsen, T., and Komuniecki, R. (eds). London: Academic Press, pp. 125–139.

Outten, F.W., Wood, M.J., Munoz, F.M., and Storz, G. (2003) The SufE protein and the SufBCD complex enhance SufS cysteine desulfurase activity as part of a sulfur transfer pathway for Fe-S cluster assembly in *Escherichia coli*. *J Biol Chem* 278: 45713–45719.

Putz, S., Gelius-Dietrich, G., Piotrowski, M., and Henze, K. (2005) Rubrerythrin and peroxiredoxin: two novel putative peroxidases in the hydrogenosomes of the microaerophilic protozoon *Trichomonas vaginalis*. *Mol Biochem Parasitol* 142: 212–223.

Rees, D.C., and Howard, J.B. (2000) Nitrogenase: standing at the crossroads. *Curr Opin Chem Biol* 4: 559–566.

Reeves, R.E. (1984) Metabolism of *Entamoeba histolytica* Schaudinn, 1903. *Adv Parasitol* 23: 105–142.

Regoes, A., Zourmpanou, D., Leon-Avila, G., van der Giezen, M., Tovar, J., and Hehl, A.B. (2005) Protein import, replication, and inheritance of a vestigial mitochondrion. *J Biol Chem* 280: 30557–30563.

Stanley, S.L., Jr (2003) Amoebiasis. *Lancet* 361: 1025–1034.

Sutak, R., Dolezal, P., Fiumera, H.L., Hrdy, I., Dancis, A., Delgadillo-Correa, M., *et al.* (2004) Mitochondrial-type assembly of FeS centers in the hydrogenosomes of the amitochondriate eukaryote *Trichomonas vaginalis*. *Proc Natl Acad Sci USA* 101: 10368–10373.

Takahashi, Y., and Tokumoto, U. (2002) A third bacterial system for the assembly of iron-sulfur clusters with

homologs in archaea and plastids. *J Biol Chem* 277: 28380–28383.

Tovar, J. (2007) Mitosomes of parasitic protozoa: biology and evolutionary significance. In *Origin of Mitochondria and Hydrogenosomes*. Martin, W.F., and Müller, M. (eds). Heidelberg: Springer-Verlag, pp. 277–300.

Tovar, J., Fischer, A., and Clark, C.G. (1999) The mitosome, a novel organelle related to mitochondria in the amitochondrial parasite *Entamoeba histolytica*. *Mol Microbiol* 32: 1013–1021.

Tovar, J., Leon-Avila, G., Sánchez, L.B., Sutak, R., Tachezy, J., van der Giezen, M., *et al.* (2003) Mitochondrial remnant organelles of *Giardia* function in iron-sulphur protein maturation. *Nature* 426: 172–176.

Vicente, J.B., Ehrenkaufer, G.M., Saraiva, L.M., Teixeira, M., and Singh, U. (2009) *Entamoeba histolytica* modulates a complex repertoire of novel genes in response to oxidative and nitrosative stresses: implications for amebic pathogenesis. *Cell Microbiol* 11: 51–69.

Weinberg, M.V., Jenney, F.E., Jr., Cui, X., and Adams, M.W. (2004) Rubrerythrin from the hyperthermophilic archaeon *Pyrococcus furiosus* is a rubredoxin-dependent, iron-containing peroxidase. *J Bacteriol* 186: 7888–7895.

Supporting information

Additional Supporting Information may be found in the online version of this article:

Fig. S1. Immunoblot analysis of ectopic expression of epitope- or GFP-tagged NifS and NifU. Blots were reacted with anti-EhNifS (A), anti-EhNifU (B), anti-Myc (C) or anti-HA antibody (D). Lanes are: 1, molecular markers; 2, Myc control transformant; 3, Myc-NifS; 4, HA control; 5, HA-NifU; 6, MycGFP; 7, MycGFP-NifU; 8, Myc-NifS/HA-NifU; 9, Myc-NifS/MycGFP-NifU.

Fig. S2. Growth kinetics of the wild-type and transgenic *E. histolytica* lines. Trophozoites from wild-type, Myc- and HA-control transformants as well as HA-NifU, Myc-NifS and Myc-NifS/HA-NifU transgenic parasite lines were seeded at initial densities of 1 10^4 ml^{-1} in 6 ml glass tubes containing BI-S-33 growth medium. Cells were counted daily using a hemocytometer; mean values and standard errors of the mean are plotted.

Please note: Wiley-Blackwell are not responsible for the content or functionality of any supporting materials supplied by the authors. Any queries (other than missing material) should be directed to the corresponding author for the article.

Molecular & Biochemical Parasitology 170 (2010) 100–104

Contents lists available at ScienceDirect

Molecular & Biochemical Parasitology

Short communication

Characterization of two isotypes of L-threonine dehydratase from *Entamoeba histolytica*☆

Afzal Husain[a,b], Ghulam Jeelani[a,c], Dan Sato[c,d], Vahab Ali[b,1], Tomoyoshi Nozaki[a,*]

[a] Department of Parasitology, National Institute of Infectious Diseases, 1-23-1 Toyama, Shinjuku-ku, Tokyo 162-8640, Japan
[b] Department of Parasitology, Gunma University Graduate School of Medicine, Maebashi, Gunma 371-8511, Japan
[c] Center for Integrated Medical Research, School of Medicine, Keio University, Shinjuku, Tokyo 160-8582, Japan
[d] Institute for Advanced Biosciences, Keio University, Tsuruoka, Yamagata 997-0052, Japan

ARTICLE INFO

Article history:
Received 14 August 2009
Received in revised form 2 November 2009
Accepted 12 November 2009
Available online 18 November 2009

Keywords:
Amino acid
Metabolism
Serine
Threonine
Anaerobic protozoa

ABSTRACT

The genome sequence of the enteric protozoan parasite *Entamoeba histolytica* suggests that amino acid catabolism plays an important role in energy metabolism. In the present study, we described kinetic and regulatory properties of catabolic L-threonine and L-serine dehydratase (TD) from *E. histolytica*. TD catalyses the pyridoxal phosphate-dependent dehydrative deamination of L-threonine and L-serine to ammonia and keto acids (2-oxobutyrate and pyruvate, respectively). *E. histolytica* possesses two TD isotypes (EhTD1-2) showing 38% mutual identity, a calculated molecular mass of 45.0 or 46.5 kDa, and an isoelectric point of 6.68 or 5.88, respectively. Only EhTD1 showed L-threonine and L-serine dehydrative deaminating activities whereas EhTD2, in which the amino acid residues involved in the substrate and cofactor binding were not conserved, was devoid of these activities. The k_{cat}/K_m value of EhTD1 was >3 fold higher for L-threonine than L-serine. EhTD1 was inhibited by L-cysteine in a competitive manner with the K_i values of 1.1 mM and 2.2 mM for L-serine and L-threonine, respectively. EhTD1 was insensitive to the allosteric activation by AMP or CMP. Three major substitutions of EhTD1 likely attribute to the insensitivity. EhTD1 was also inhibited about 50% by 20 mM 2-oxobutyrate, pyruvate, and glyoxylate; the inhibition was not, however, reversed by AMP. Together, these data showed that EhTD1 possesses unique regulatory properties distinct from other organisms and may play an important role in energy metabolism via amino acid degradation in *E. histolytica*.

L-threonine dehydratase (TD, EC 4.3.1.19) belongs to the systematic subclass of ammonia lyases (EC 4.3.1), and catalyzes deamination of L-threonine to yield ammonia and 2-oxobutylate (Fig. 1A) via an intermediary dehydration [1]. The enzyme from a number of sources also acts on L-serine to yield pyruvate [1]. Most TDs have been shown to contain pyridoxal phosphate (PLP) as a prosthetic group, forming a Schiff base with the ε-amino moiety of a specific lysyl residue [2]. These dehydratases may serve catabolic or biosynthetic purposes and hence are ubiquitous. Biosynthetic TD catalyzes the first reaction in the isoleucine biosynthetic pathway. In all biosynthetic TDs studied so far, isoleucine or valine is the negative or positive allosteric effector, respectively [3]. Catabolic TD catalyzes the first reaction in the anaerobic breakdown of L-threonine to propionate [4]. Catabolic TD is insensitive to L-isoleucine and L-valine and activated by AMP [4].

E. histolytica, the causative agent of human amoebiasis, is an enteric protozoan parasite and causes amoebic colitis and extra intestinal abscesses [5]. *E. histolytica*, like other anaerobic or microaerophilic parasitic protozoa such as *Giardia lamblia* and *Trichomonas vaginalis*, lacks features of eukaryotic aerobic metabolism including the tricarboxylic acid (TCA) cycle and oxidative phosphorylation, and energy generation is primarily by substrate level phosphorylation [6]. Glycolysis under anaerobic conditions can use only part of the energy contained in glucose for ATP generation. The *E. histolytica* genome sequence suggests that ATP can be generated from amino acids [7]. This finding is further supported by the fact that *E. histolytica* trophozoites grown in axenic medium take up several amino acids when glucose is not available [8]. Amino acid degradation can produce either pyruvate or other 2-keto acids (Fig. 1A). Pyruvate:ferredoxin oxidoreductase (PFOR) is known to have a relaxed specificity. PFOR oxidatively decarboxylates pyru-

Abbreviations: TD, threonine dehydratase; EhTD, *Entamoeba histolytica* threonine dehydratase; PLP, pyridoxal 5′-phosphate; CMP, cytosine monophosphate; PCR, polymerase chain reaction.

☆ *Note:* The nucleotide sequence data of *Entamoeba histolytica* TD1 and TD2 reported in this paper are available at the DDBJ/GenBank®/EBI data bank with accession numbers AB511882 and AB511883.

* Corresponding author. Tel.: +81 3 5285 1111x2600; fax: +81 3 5285 1219.
E-mail address: nozaki@nih.go.jp (T. Nozaki).
[1] Present address: Department of Biochemistry, Rajendra Memorial Research Institute of Medical Sciences, Agamkuan, Patna 800007, India.

0166-6851/$ – see front matter © 2009 Elsevier B.V. All rights reserved.
doi:10.1016/j.molbiopara.2009.11.004

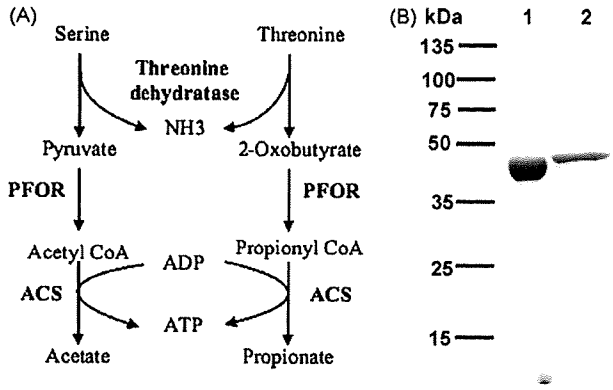

Fig. 1. (A) Presumed pathways of threonine and serine catabolism in *E. histolytica*. Abbreviations are: PFOR, pyruvate:ferredoxin oxidoreductase; ACS, acetyl CoA synthetase. (B) SDS-PAGE analysis of purified rEhTD1 and rEhTD2. Samples were electrophoresed on a 12.0% polyacrylamide gel and stained with Coomassie brilliant blue. Lanes 1 and 2 showed rEhTD1 and rEhTD2, respectively, eluted with 200 mM imidazole and dialyzed.

vate and 2-oxobutyrate to generate acetyl CoA and propionyl CoA, respectively [9]. Acetyl CoA synthetase (ACS), which is responsible for generating ATP via acetyl-CoA hydrolysis, also accepts propionyl-CoA as a substrate [10], completing the proposed pathway for ATP generation from various amino acids (Fig. 1A).

It was shown that L-serine and L-threonine are incorporated by *E. histolytica* trophozoites in the presence or absence of glucose [8]. It was also demonstrated that addition of L-serine to the culture medium stimulates oxygen consumption [11]. While the fate of L-serine and L-threonine after incorporation and the mechanisms of the augmented oxygen consumption by L-serine remain unknown, these facts indeed suggest the importance of serine metabolism in the *E. histolytica* energy production. In the present study, we have characterized for the first time, catabolic TD in trophozoites of an axenic HM-1:IMSS cl6 strain of *E. histolytica* [12].

We identified three genes encoding TD isotypes by homology search against the *E. histolytica* genome database [7] using TD protein sequences from bacteria, plants, and mammals. Since the third TD isotype (EHI_126080) is almost identical (98%) to the first TD (EHI_092390) with only a few amino acid changes at the amino and carboxyl termini of the protein, we did not further analyze the third TD. We accordingly designated the first and second putative TD genes as *EhTD1* and *EhTD2* [corresponding to EHI_092390 (AB511882) and EHI_049910 (AB511883)], respectively. Each of *EhTD1* and *EhTD2* genes contains a 1272-bp and 1290-bp open reading frame, which encodes the protein of 423 and 429 amino acid residues with a predicted molecular mass of 45.0 and 46.5 kDa, and pI of 6.68 and 5.88, respectively. The amino acid sequence of EhTDs showed 20–49% identities to TDs from archaea, bacteria, animals, and plants. EhTD1 and EhTD2 showed highest amino acid identities to TDs from an anaerobic thermohalophilic *Halothermothrix orenii* and a thermophilic uncultivable bacterium, dependent on microbial commensalism, *Symbiobacterium thermophilum* (49% and 38%, respectively). The identity between EhTD1 and EhTD2 was only 38%. Both EhTDs were devoid of the amino-terminal transit peptide, which suggests that amoebic TD genes encode cytosolic proteins.

A multiple alignment of EhTD isotypes with *Salmonella typhimurium* TD, by the Clustal W program (http://clustalw.ddbj.nig.ac.jp/top-e.html), showed that most of the important residues implicated in substrate and cofactor binding, as predicted from the crystal structure of *S. typhimurium* TD, were well conserved in EhTD1. However, there were a few substitutions of the amino acids for substrate binding: Tyr-153, Cys-238, and Ala-284 of *S. typhimurium* TD to Phe-169, Ile-254, and Ser-300 in EhTD1 [4], respectively (Fig. 2, "A"). In contrast, there were more substitutions in EhTD2 compared to EhTD1. In EhTD2, Pro-152, Tyr-153, Gln-162, Gly-237, and Cys-238 of *S. typhimurium* TD were substituted with Ala-175, Arg-176, Asp-185, Thr-260, and Asp-261, respectively ("B"). The tetraglycine loop, which is involved in the formation of hydrogen bonds with the phosphate moiety of PLP [4], was conserved in EhTD1, whereas the residues in the loop were partially altered in EhTD2 (Ser-208 and Ser-210, "C"). Among the amino acid residues involved in the binding of CMP and AMP, EhTD1 showed a few substitutions of Arg-53, Asp-119, and Gln-275 of *S. typhimurium* TD to Lys-69, Gly-135, and Glu-291 in EhTD1, respectively "D"). EhTD2 was devoid of the residues required for AMP and CMP binding, except for Tyr-143, Lys-301, and Asn-336, corresponding to Tyr-120, Lys-278, and Asn-314 of *S. typhimurium* TD (substituted residues are marked "E"). Phylogenetic analysis of EhTDs with TD protein sequences from various organisms did not clearly indicate the source of the amebic TD, but suggested that *E. histolytica* TDs were not obtained by lateral gene transfer (data not shown). EhTDs form a well-supported clade with catabolic TDs, but not with biosynthetic TDs from other organisms, which suggests the absence of biosynthetic TDs and isoleucine/valine biosynthetic pathway in *E. histolytica*.

To demonstrate enzymatic properties of the putative EhTD proteins, the recombinant EhTD1 and 2 were produced by prokaryotic expression system. The open reading frame of the individual TD genes was PCR amplified using *E. histolytica* cDNA library [13], platinum pfx DNA polymerase (Life Technologies, Tokyo, Japan), and oligonucleotide primers: 5′-cctCATATGacagagggaagtgaatactt-3′ and 5′-ccaGGATCCttacttgaaaacatatccagc-3′ (EhTD1); 5′-cctCATATGagtgacgtagaagttcctgca-3′ and 5′-ccaGGATCCttagacaaagacaaattcata-3′ (EhTD2), where capital letters indicate *Nde*I and *Bam*HI restriction sites. The PCR fragments were digested with *Nde*I and *Bam*HI, electrophoresed, purified with Geneclean kit II (BIO 101, Vista, CA, USA), and cloned into *Nde*I and *Bam*HI-double-digested pCold1 (Takara, Tokyo, Japan) to produce pCold1-EhTD1 and pCold1-EhTD2. *Escherichia coli* BL21 (DE3) cells (Takara) were transformed by one of these plasmids and grown in LB medium containing 50 μg/ml ampicillin with 1 mM of isopropyl β-D-thio galactopyranoside at 15 °C for 24 h. *E. coli* cells were harvested, washed with PBS, pH 7.4, lysed and centrifuged at 25,000 × *g* for 15 min at 4 °C. The supernatant containing N-terminal histidine-tagged EhTD1 or EhTD2 was purified with Ni^{2+}-NTA His-bind resin (Life Technologies). The purity of products was assessed to be >95% by SDS polyacrylamide gel electrophoresis stained with Coomassie brilliant blue (Fig. 1B).

TD activity was measured on the basis of the production of α-keto acids. The amount of α-keto acids generated was determined either colorimetrically [14] or spectrophotometrically at 310 nm [15]. Both rEhTD1 and rEhTD2 showed specific PLP peaks at 413 nm, suggesting the presence of PLP as a prosthetic group. The maximum activity of rEhTD1 was observed at slightly basic pH (8.5–9.0). The inclusion of 2 mM dithiothreitol in the reaction mixture enhanced enzymatic activity by >2 fold. EDTA at 1 mM also slightly enhanced activity. Unlike rEhTD1, rEhTD2 was devoid of putative serine dehydratase or TD activity under the conditions aforementioned. The lack of TD activity in EhTD2 may be attributable to the improper folding due to prokaryotic expression system or to the absence of the amino acid residues known to be involved in substrate and cofactor binding. We also examined whether 20 amino acids and 12 related compounds are degraded by rEhTD2, by incubating the mixture of potential substrates with rEhTD2, followed by measuring the concentrations of the substrates and their products by capillary electrophoresis-mass spectrometry [16]. However, we were unable to detect any degraded compounds (data not shown).

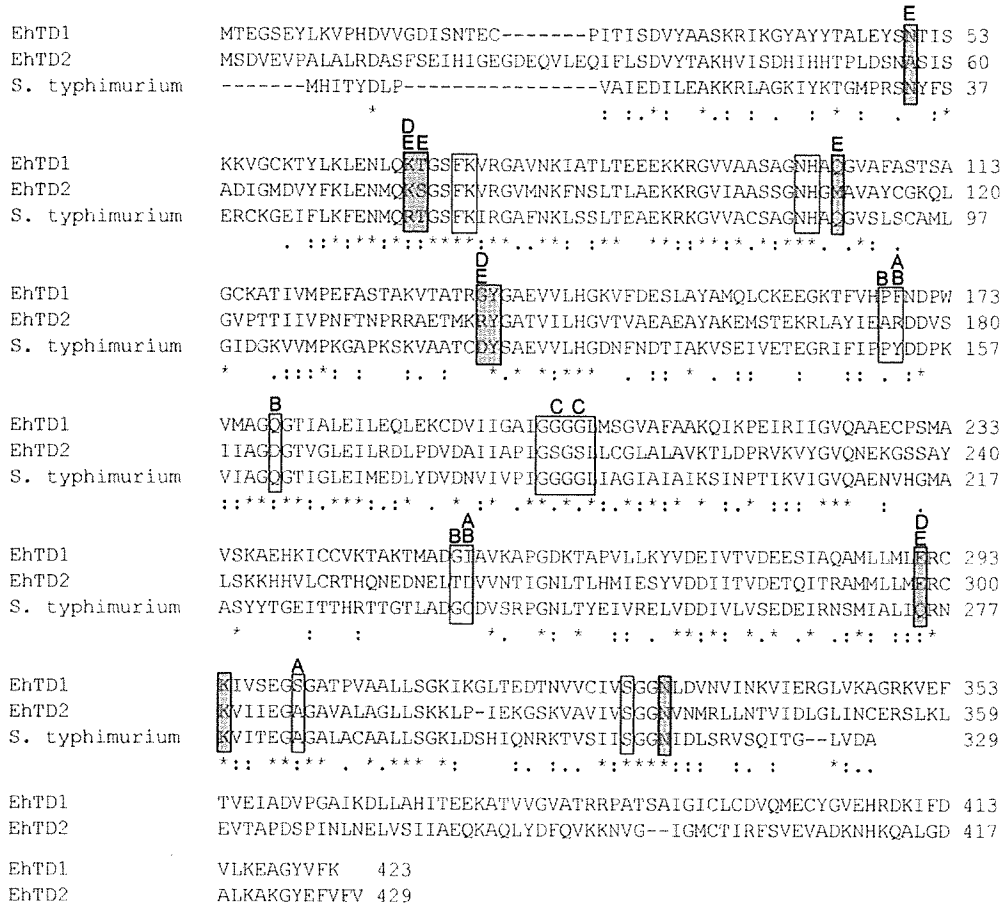

Fig. 2. Sequence alignment of threonine dehydratase from *E. histolytica* and *S. typhimurium*. Two *E. histolytica* (EhTD1 and EhTD2) and *S. typhimurium* (NP_462158) sequences were aligned using the CLUSTAL W program. Dashes indicate gaps. The highly conserved residues known to participate in the binding to substrates and PLP on the basis of crystal structures of *S. typhimurium* TD [4] are shown in open boxes, whereas the residues involved in AMP/CMP binding are shown in shaded boxes. Substituted amino acids in the substrate binding domains of EhTD1 and EhTD2 are depicted by "A" and "B", respectively, while those in the PLP binding domains of EhTD2 are depicted by "C". Substituted amino acids in the AMP/CMP binding domains of EhTD1 and EhTD2 are depicted by "D" and "E", respectively.

The K_m and k_{cat} values of rEhTD1 for L-serine and L-threonine were significantly different (Table 1). At saturating concentrations of substrates, rEhTD1 showed an approximately 2 fold higher affinity for L-threonine than L-serine. The k_{cat} of rEhTD1 was also 1.7-fold higher for L-threonine than L-serine. EhTD1 showed a ~3 fold higher k_{cat}/K_m value for L-threonine than L-serine, suggesting that EhTD1 primarily acts on L-threonine to generate 2-oxobutyrate, and also utilizes serine, at higher concentrations, to generate pyruvate. The premise that EhTD1 functions at relatively high L-serine concentrations was further supported by the previous study showing that serine supplementation to the culture medium caused increased oxygen consumption, most probably by increased synthesis of pyruvate [11]. The intracellular concentrations of L-serine and L-threonine under *in vitro* culture conditions are 3.2 and 4.5 mM, respectively [17]. Thus, EhTD1 preferentially degrades L-threonine, but not L-serine unless its kinetic properties are modulated by unknown factors and mechanisms *in vivo*. We also tested structurally related amino acids (L-homoserine, *O*-phospho-L-serine, *O*-acetyl-L-serine, *N*-acetyl-L-serine, *O*-succinyl-L-homoserine, and cystathionine) as substrates, but no activity was observed against these substrates.

The effect of L-cysteine and DL-homocysteine on the activity of rEhTD1 was examined. Like TDs from bacteria, animals, and plants [18], rEhTD1 was also inhibited by L-cysteine, but no significant inhibition was observed by DL-homocysteine up to 4 mM. Double reciprocal plots in the presence or absence of L-cysteine, showed that EhTD1 is inhibited by L-cysteine at physiological concentrations (K_i, 1.1 and 2.2 mM for L-serine and L-threonine, respectively), similar to the TDs from other organisms [19]. The inhibition by L-cysteine was more prominent when L-serine is used as a substrate

Table 1
Kinetic parameters of recombinant *E. histolytica* TD1.

Substrate	K_m (mM)	k_{cat} (s^{-1})	k_{cat}/K_m	K_i (mM) for L-cysteine	Mode of inhibition
L-serine	13.5 ± 0.8	3.0 ± 0.5	0.2 ± 0.1	1.1 ± 0.2	Competitive
L-threonine	7.3 ± 1.7	5.2 ± 0.2	0.7 ± 0.1	2.2 ± 0.4	Competitive

Assays were carried out in 100 μL of 100 mM Tris/HCl buffer (pH 9.0) containing 2 mM dithiothreitol, 1 mM EDTA, and 50 μM PLP, and 1–2 μg of the recombinant enzymes, at 37 °C for 20 min. The amount of α-keto acids generated was quantitated as described previously [14]. The L-serine and L-threonine concentrations ranging 1–64 mM were used to determine of kinetic parameters. To determine the K_i value for L-serine or L-threonine, the constant concentration (40 mM) of L-threonine or L-serine was used. All values are expressed as a mean ± S.E. of triplicates.

Table 2
Inhibition of recombinant EhTD1 by keto-acids.

	%Inhibition	
	Without AMP	With 5 mM AMP
Pyruvate	45.3 ± 1.7	44.6 ± 0.2
Glyoxylate	54.1 ± 1.2	49.6 ± 2.7
2-Oxobutyrate	49.3 ± 1.1	43.2 ± 3.8

TD activity was measured spectrophotometrically at 310 nm as described previously [15]. Effects of 20 mM of various keto acids (pyruvate, 2-oxobutyrate or glyoxylate) on the activity of rEhTD1 in the presence or absence of AMP (5 mM). TD activity is shown in percentage relative to that of TD activity measured in the absence of both keto acid and AMP. All values are expressed as a mean ± S.E. of triplicates.

(Table 1). Therefore, L-cysteine likely plays a role in the regulation of EhTD1, particularly serine dehydratase activity of EhTD1 at physiological concentrations. We also studied the effect of ATP, ADP, AMP, and CMP on the activity of rEhTD1. All of these nucleotides have been shown to be allosteric regulators of catabolic TDs from various sources [4]. rEhTD1 was inhibited by ATP in a dose-dependent manner (data not shown). It showed approximately 50% inhibition by 10 mM of ATP. In contrast to the catabolic TDs from bacteria plants and animals [4,15], rEhTD1 was insensitive to the allosteric activation by ADP, AMP, and CMP (data not shown). The AMP/CMP binding site of EhTD1 has three substitutions of Arg-53 to Lys-69, Asp-119 to Gly-135, and Gln-275 to Glu-291 (Fig. 2, "D"). The guanidium group of Arg-53 forms a hydrogen bond with the phosphate group of AMP or CMP. The side-chain oxygen atom of Asp-119 is hydrogen bonded to the N4 atom of the adenine moiety of AMP or the N3 atom of the cytosine moiety of CMP, whereas the side-chain oxygen atom of Gln-275 is involved in the hydrogen bonding with the N6 atom of the adenine moiety of AMP or the O2 atom of the cytosine moiety of CMP [4]. Absence of these hydrogen bonds might contribute to the lack of AMP or CMP binding to the enzyme. Allosteric activation by valine and inhibition by isoleucine were described for biosynthetic TDs [3]. However, in accordance with the catabolic nature, rEhTD1 was neither activated by valine nor inhibited by isoleucine (data not shown). We also investigated the effect of various catabolites on the activity of rEhTD1 in both the presence and absence of AMP. rEhTD1 was markedly inhibited by both the end products, i.e. pyruvate and 2-oxobutyrate, and also by glyoxylate (Table 2). Inhibition by these keto acids was not reversed by 5 mM AMP, which is dissimilar to the catabolic TD from various other sources. This is in accordance with the lack of allosteric activation of EhTD1 by AMP. Inhibition of catabolic TDs by the keto acids and reversal of the inhibition by AMP have been well documented [15]. Altogether, these findings indicate that the regulatory mechanisms of EhTD1 are distinct from that of bacterial, plant, and animal counterparts.

It has been shown that TD is developmentally regulated in *Dictyostelium discoideum* [19]. *D. discoideum* has both catabolic and biosynthetic TDs, and during the development of the vegetative to pseudoplasmodial stage, biosynthetic TD activity decreases while catabolic TD is upregulated [19]. Similarly, TD is also developmentally regulated in *Entamoeba*. Our transcriptome study showed that an *E. invadens* homologue of *EhTD1* gene is down regulated by 8 fold during the transition of trophozoites to the dormant cyst stage, suggesting its role in proliferation (Escueta et al., unpublished). In *Trypanosoma brucei*, which lacks TD, L-threonine is metabolized using the alternative aminoacetone pathway, which involves a mitochondrial threonine dehydrogenase and aminoacetone synthase. This route is not operational in *E. histolytica* and *Leishmania major* [20]. *L. major* has two pathways to metabolize L-threonine. L-threonine is converted to 2-oxobutyrate by TD, and then oxidized to succinyl CoA. Alternatively, L-threonine can be converted to L-glycine by serine hydroxymethyltransferase (SHMT). The resulting L-glycine can be converted to pyruvate via L-serine by the action of SHMT and TD. The later route of threonine catabolism does not operate in *Entamoeba* as a gene encoding SHMT is absent [7]. In *T. vaginalis*, which possesses TD, L-threonine and L-serine are also used for energy generation in the absence of carbohydrates [21]. In summary, we have characterized TD, one of the key enzymes that allow utilization of amino acids as energy source [22,23], from *E. histolytica*. Our findings should help to understand the significance of the amino acid catabolism for energy generation in *E. histolytica* [24].

Acknowledgements

We thank Kumiko Nakada-Tsukui, Fumika Mi-ichi, and all other members of our laboratory for the technical assistance and valuable discussions. This work was supported by a Grant-in-Aid for Scientific Research from the Ministry of Education, Culture, Sports, Science and Technology of Japan to T.N. (18GS0314, 18050006, 18073001), a grant for research on emerging and re-emerging infectious diseases from the Ministry of Health, Labour and Welfare of Japan (H20-Shinkosaiko-016), and a grant for research to promote the development of anti-AIDS pharmaceuticals from the Japan Health Sciences Foundation to T.N.

References

[1] Umbarger HE. Threonine deaminases. Adv Enzymol 1973;37:349–95.
[2] Phillips AT, Wood WA. The mechanism of action of 5′-adenylic acid-activated threonine dehydratase. J Biol Chem 1965;240:4703–9.
[3] Umbarger HE. Evidence for a negative feedback mechanism in the biosynthesis of isoleucine. Science 1956;123:848.
[4] Simanshu DK, Savithri HS, Murthy MRN. Crystal structures of *Salmonella typhimurium* biodegradative threonine deaminase and its complex with CMP provide structural insights into ligand-induced oligomerization and enzyme activation. J Biol Chem 2006;281:39630–41.
[5] World Health Organization/Pan American Health Organization Report. A consultation with experts on amebiasis. Epidemiological Bulletin/PAHO 1997;18:13–4.
[6] Müller M. Enzymes and compartmentation of core energy metabolism of anaerobic protists—a special case in eukaryotic evolution. In: Coombs GH, Vickerman K, Sleigh MA, Warren A, editors. Evolutionary Relationships Among Protozoa. Dordrecht, The Netherlands: Kluwer Academic Publishers; 1998. p. 109–32.
[7] Loftus B, Anderson I, Davies R, et al. The genome of the protist parasite *Entamoeba histolytica*. Nature 2005;433:865–8.
[8] Zuo X, Coombs GH. Amino acid consumption by the parasitic, amoeboid protists *Entamoeba histolytica* and *E. invadens*. FEMS Microbiol Lett 1995;130:253–8.
[9] Samarawickrema NA, Brown DM, Upcroft JA, Thammapalerd N, Upcroft P. Involvement of superoxide dismutase and pyruvate:ferredoxin oxidoreductase in mechanisms of Metronidazole resistance in *Entamoeba histolytica*. J Antimicrobial Chemother 1997;40:833–40.
[10] Reeves RE, Warren LG, Susskind B, Lo HS. An energy-conserving pyruvate-to-acetate pathway in *Entamoeba histolytica*. Pyruvate synthase and a new acetate thiokinase. J Biol Chem 1977;252:726–31.
[11] Takeuchi T, Weinbatch EC, Gottlieb M, Diamond LS. Mechanism of L-serine oxidation in *Entamoeba histolytica*. Comp Biochem Physiol B 1979;62:281–5.
[12] Diamond LS, Harlow DR, Cunnick CC. A new medium for the axenic cultivation of *Entamoeba histolytica* and other *Entamoeba*. Trans R Soc Trop Med Hyg 1978;72:431–2.
[13] Nozaki T, Asai T, Kobayashi S, et al. Molecular cloning and characterization of the genes encoding two isoforms of cysteine synthase in the enteric protozoan parasite, *Entamoeba histolytica*. Mol Biochem Parasitol 1998;97:33–44.
[14] Soda K. Microdetermination of D-amino acids and D-amino acid oxidase activity with 3-methyl-2-benzothiazolone hydrazone hydrochloride. Anal Biochem 1968;25:228–35.
[15] Shizuta Y, Kurosawa A, Inoue K, Tanabe T, Hayaishi O. Regulation of biodegradative threonine deaminase. I. Allosteric inhibition of the enzyme by a reaction product and its reversal by adenosin 5′-monophosphate. J Biol Chem 1973;248(2):512–20.
[16] Saito N, Robert M, Kochi H, et al. Metabolite profiling reveals YihU as a novel hydroxybutyrate dehydrogenase for alternative succinic semialdehyde metabolism in *Escherichia coli*. J Biol Chem 2009;284:16442–51.
[17] Bakker Grunwald T, Martin JB, Klein G. Characterization of glycogen and amino acid pool of *Entamoeba histolytica* by 13C-NMR spectroscopy. J Eukaryot Microbiol 1995;42:346–9.

[18] Leoncini R, Pagani R, Marinello E, Keleti T. Double inhibition of L-threonine dehydratase by aminothiols. Biochim Biophys Acta 1989;994:52–8.
[19] Pong SS, Loomis Jr WF. Replacement of an anabolic threonine deaminase by a catabolic threonine deaminase during development of *Dictyostelium discoideum*. J Biol Chem 1973;248:4867–73.
[20] Opperdoes F, Coombs GH. Metabolism of *Leishmania*; proven and predicted. Trends Parasitol 2007;23:149–58.
[21] Zuo X, Lockwood BC, Coombs GH. Uptake of amino acids by the parasitic, flagellated protist *Trichomonas vaginalis*. Microbiology 1995;141:2637–42.
[22] Tokoro M, Asai T, Kobayashi S, Takeuchi T, Nozaki T. Identification and characterization of two isoenzymes of methionine γ-lyase from *Entamoeba histolytica*. J Biol Chem 2003;278:42717–27.
[23] Sato D, Yamagata W, Harada S, Nozaki T. Kinetic characterization of methionine γ-lyases from the enteric protozoan parasite *Entamoeba histolytica* against physiological substrates and trifluoromethionine, a promising lead compound against amoebiasis. FEBS J 2008;275:548–60.
[24] Nozaki T, Ali V, Tokoro M. Sulfur-containing amino acid metabolism in parasitic protozoa. Adv Parasitol 2005;60:1–99.

International Journal for Parasitology xxx (2010) xxx–xxx

Contents lists available at ScienceDirect

International Journal for Parasitology

journal homepage: www.elsevier.com/locate/ijpara

Members of the *Entamoeba histolytica* transmembrane kinase family play non-redundant roles in growth and phagocytosis

Sarah N. Buss [a,*], Shinjiro Hamano [b], Alda Vidrich [c], Clive Evans [d], Yan Zhang [d], Oswald R. Crasta [d], Bruno W. Sobral [d], Carol A. Gilchrist [e], William A. Petri Jr. [e]

[a] Department of Microbiology, University of Virginia, Charlottesville, VA 22908-1340, USA
[b] Department of Parasitology, Institute of Tropical Medicine (NEKKEN) and the Global COE Program, Nagasaki University, Nagasaki 852-8523, Japan
[c] Digestive Health Center of Excellence, Department of Medicine, University of Virginia, Charlottesville, VA 22908-1340, USA
[d] Virginia Bioinformatics Institute, Blacksburg, Virginia, 24061-0477, USA
[e] Division of Infectious Diseases and International Health, Departments of Internal Medicine, Microbiology and Pathology, University of Virginia, Charlottesville, VA 22908-1340, USA

ARTICLE INFO

Article history:
Received 13 November 2009
Received in revised form 15 December 2009
Accepted 17 December 2009
Available online xxxx

Keywords:
Entamoeba histolytica
Transmembrane kinase
Phagocytosis
Lectin
Laser-capture microdissection

ABSTRACT

Entamoeba histolytica contains a large and novel family of transmembrane kinases (TMKs). The expression patterns of the *E. histolytica* TMKs in individual trophozoites and the roles of the TMKs for sensing and responding to extracellular cues were incompletely characterised. Here we provide evidence that single cells express multiple TMKs and that TMK39 and TMK54 likely serve non-redundant cellular functions. Laser-capture microdissection was used in conjunction with microarray analysis to demonstrate that single trophozoites express more than one TMK gene. Anti-peptide antibodies were raised against unique regions in the extracellular domains of TMK39, TMK54 and PaTMK, and TMK expression was analysed at the protein level. Flow cytometric assays revealed that populations of trophozoites homogeneously expressed TMK39, TMK54 and PaTMK, while confocal microscopy identified different patterns of cell surface expression for TMK39 and TMK54. The functions of TMK39 and TMK54 were probed by the inducible expression of dominant-negative mutants. While TMK39 co-localised with ingested beads and expression of truncated TMK39 interfered with trophozoite phagocytosis of apoptotic lymphocytes, expression of a truncated TMK54 inhibited growth of amoebae and altered the surface expression of the heavy subunit of the *E. histolytica* Gal/GalNAc lectin. Overall, our data indicates that multiple members of the novel *E. histolytica* TMK family are utilised for non-redundant functions by the parasite.

1. Introduction

Cell surface receptors mediate the response to the environment across all forms of life. In metazoan organisms and plants, transmembrane kinases (TMKs) make up one of the major classes of cell surface receptors, with humans encoding about 80 TMKs (Manning et al., 2002) and *Arabidopsis thaliana* encoding over 400 (Champion et al., 2004; Shiu et al., 2004). The paradigm of receptor-mediated signalling governing cellular responses to environmental cues in plants and metazoa has not been fully extended to protozoa because protozoa have a general paucity of TMKs. However, examples of protozoan TMKs are beginning to be discovered and include nine predicted TMKs in *Dictyostelium discoideum* (Goldberg et al., 2006), 10 potential TMKs in *Trypanosoma brucei* (Parsons et al., 2005), 11 putative TMKs in *Plasmodium* (Ward et al., 2004), 88 predicted TMKs in *Monosiga brevicollis* (King and Carroll, 2001; Manning et al., 2008) and over 90 novel TMKs predicted in the protozoan parasite *Entamoeba histolytica* (Beck et al., 2005). The significance of these proteins remains unclear, as the majority have been characterised by sequence analysis only. A more complete understanding of protozoan TMKs will help define the mechanisms that these organisms use to respond to their environment and may shed light on the evolution of eukaryotic protein kinases.

The large family of novel TMKs identified in the *E. histolytica* genome has proposed roles in both amoebic response to the environment and immune evasion (Beck et al., 2005). *E. histolytica* is the causative agent of amoebiasis, a disease responsible for significant morbidity and mortality worldwide (WHO/PAHO/UNESCO, 1997). The parasite's biphasic life cycle consists of transmissible cysts and replicating trophozoites that colonise the lumen of the large intestine and occasionally invade the mucosa. Trophozoites must survey and adapt to the complex intestinal milieu and evade the immune system, but mechanisms that regulate the parasite's ability to persist for months within its human host remain incompletely understood.

* Corresponding author. Address: Division of Infectious Diseases and International Health, University of Virginia Health System, Carter Harrison Building Room 1711, 345 Crispell Drive, Charlottesville, VA 22908-1340, USA. Tel.: +1 434 924 8189; fax: +1 434 924 0075.
E-mail address: snb4k@virginia.edu (S.N. Buss).

0020-7519/$36.00 © 2010 Australian Society for Parasitology Inc. Published by Elsevier Ltd. All rights reserved.
doi:10.1016/j.ijpara.2009.12.007

Please cite this article in press as: Buss, S.N., et al. Members of the *Entamoeba histolytica* transmembrane kinase family play non-redundant roles in growth and phagocytosis. Int. J. Parasitol. (2010), doi:10.1016/j.ijpara.2009.12.007

In protozoan parasites such as *Giardia lamblia*, *Plasmodium falciparum* and *T. brucei*, antigenic variation, or the alteration of immunodominant surface antigens, is a common mechanism used to subvert host defences (Adam et al., 1988; Su et al., 1995; Stockdale et al., 2008). The process requires three elements: a large gene family encoding antigenically distinct surface proteins, expression of one variant antigen at a time by a single pathogen and a mechanism to switch the expressed gene (Borst and Genest, 2006). The *E. histolytica* TMKs have been implicated in the process of antigenic variation due to the nature of the gene family, the course of amoebic infection and observations made during transcriptional profiling studies (Beck et al., 2005). Additionally, some *E. histolytica* TMKs share sequence similarity with the variant-specific surface proteins (VSP) that are involved in the process of antigenic variation in *G. lamblia* (Beck et al., 2005).

It is possible that *Entamoeba* trophozoites undergo antigenic variation, as prolonged *E. histolytica* infections do occur (Haque et al., 2002) and antibody mediated protective immunity against *Entamoeba* is incomplete (Haque et al., 2001). However, trophozoites are known to use the process of capping, whereby antibody–antigen complexes are concentrated and released from the cell surface, as a means to avoid immune attack (Calderón et al., 1980). Additionally, amoebic trophozoites directly kill and ingest host cells, providing the organism with another mechanism for immune evasion (Ravdin et al., 1980). Nonetheless, it remains possible that the unusual TMK family may be involved with the process of antigenic variation. Real time PCR analysis of TMK expression by trophozoites during growth in culture revealed temporal changes in expression levels of some TMKs (Beck et al., 2005). As antigenic variation is known to occur without immune pressure (Roberts et al., 1992), the observed changes could be indicative of an antigenic switching event, where the averaging of population data masked expression of a single TMK by each cell.

Changes in TMK expression levels could also indicate that TMKs have specialised functions, as the TMKs have also been proposed to represent a major receptor system used by the cell to sense and respond to extracellular cues. The structural organisation of the *E. histolytica* TMKs suggests that they are type 1 integral membrane proteins, with signal-peptides, receptor-like extracellular domains and intracellular kinase domains, phylogenetically related to both S/T and Y kinases (Beck et al., 2005). When the TMKs were divided into nine sub-groups (A, B_{1-3}, C, D_{1-2}, E and F) based on signature motifs found within the substrate recognition regions of their kinase domains, similarity in the extracellular domains became apparent within sub-groups with respect to the size and the distribution of cysteine-rich motifs, suggesting that TMK sub-groups represent functionally distinct receptor families with sub-family-specific substrates and ligands (Beck et al., 2005). However, only two TMKs have been partially characterised to date: PaTMK (TMK-96, sub-family B_3) is expressed at the cell surface and functions in erythrophagocytosis (Boettner et al., 2008) and members of the B_1 family of TMKs play a role in proliferation and sensitivity to serum-derived growth factors (Mehra et al., 2006).

In this study, we sought to determine whether TMKs represent a gene family that undergoes antigenic variation or are an example of a protozoan TMK family that likely represents a major cell surface receptor system. We used laser-capture microdissection (LCM) and single cell microarray analysis and determined that a single amoeba expresses more than one TMK. To confirm expression of some TMKs at the protein level, anti-peptide antibodies were developed against TMK39 and TMK54. These TMKs were chosen because microarray data previously indicated that the genes were highly transcribed (amongst the TMKs) in both cultured and animal passaged trophozoites (Gilchrist et al., 2006), and TMK39 was identified at an early time point in a phagosomal proteome (Okada et al., 2006). We used the anti-peptide antibodies to stain cells for flow cytometric analysis and determined that the TMKs were homogenously expressed by trophozoites within a population. The antibodies were also used to localise TMK39 and TMK54 to discrete regions of the amoebic plasma membrane. We then utilised a functional genetic approach to demonstrate that TMK39 and TMK54 likely serve non-redundant cellular functions.

2. Materials and methods

2.1. Cultivation of E. histolytica and LCM

E. histolytica trophozoites, strain HM-1:IMSS, were grown axenically at 37 °C in complete TYI-S-33 medium containing 100 U/ml of penicillin and 100 μg/ml streptomycin (Invitrogen, Carlsbad, CA, USA) (Diamond, 1961). For all experiments, trophozoites were harvested during log-phase growth by a 10 min incubation on ice. For LCM analysis, harvested trophozoites were allowed to adhere to PEN foil-coated glass slides specifically designed for laser microdissection (Leica Microsystems, Bannockburn, IL, USA) for 15 min at 37 °C in TYI-S-33 media. Adherent trophozoites were sequentially fixed for 5 min in 70% and 100% ethanol followed by a few dips in xylene to completely dehydrate the samples and air-dried. Subsequently, single cells were captured from the PEN slides using the Leica AS LMD microdissection system (Leica Microsystems, Bannockburn, IL, USA). Captured cells were immediately processed as described below.

2.2. RNA isolation, amplification and microarray hybridization

RNA was purified from a single amoeba using the PicoPure™ RNA Isolation Kit (Molecular Devices, Sunnyvale, CA, USA) and the WT-Ovation™ Pico System (NuGEN, San Carlos, CA, USA) was used for cDNA synthesis and amplification. The quantity of cDNA obtained from one amplification cycle was insufficient for microarray analysis. Therefore one cycle amplified cDNA (1C) was subjected to a second cycle of amplification. Prior to microarray analysis, the linearity of the relationship between 1C and twice amplified cDNA (2C) was validated by quantitative reverse transcription PCR (qRT-PCR) (Section 2.4). 2C from a single cell was used for biotinylated cRNA synthesis. After biotinylation, 2 μg of cRNA was hybridized to the E_his-1a520285 Affymetrix custom array that has been described elsewhere (Gilchrist et al., 2006). The arrays were washed and stained with streptavidin–phycoerythrin (Molecular Probes, Carlsbad, CA, USA), following the standard Affymetrix protocol for eukaryotic targets (http://www.affymetrix.com/support/technical/manual/expression_manual.affx). The arrays were scanned with an Affymetrix Gene Chip scanner 3000 1 and Affymetrix® GeneChip® Operating Software (GCOS) (http://www.affymetrix.com/products/software/specific/gcos.affx) was used to determine the detection call (present, marginal, or absent) for each probe set. The experiment was carried out in duplicate. Additionally, raw data from the arrays were normalised at the probe level by the gcRMA algorithm and then log2 transformed (Irizarry et al., 2003). The average log intensity values for all TMKs and for a few reference genes are listed in Supplementary Table S2. The complete microarray data was deposited in NCBI's Gene Expression Omnibus (Barrett et al., 2005) and is accessible through GEO Series accession number GSE19064 (http://www.ncbi.nlm.nih.gov/geo/query/acc.cgi?acc=GSE19064).

2.3. Genome analysis and datasets

The re-annotated *E. histolytica* genome, available at http://pathema.tigr.org, (GenBank accession number AAFB00000000) was used in this analysis.

Please cite this article in press as: Buss, S.N., et al. Members of the *Entamoeba histolytica* transmembrane kinase family play non-redundant roles in growth and phagocytosis. Int. J. Parasitol. (2010), doi:10.1016/j.ijpara.2009.12.007

2.4. qRT-PCR for validation of amplification and microarray

For validation of RNA amplification procedures, RNA from 10^6 *E. histolytica* trophozoites was prepared using the PicoPure™ RNA Isolation Kit and then subjected to either one or two cycles of amplification with the WT-Ovation™ Pico System. Two rounds of amplification yielded approximately 1.67 times more RNA than one round. 1C and 2C were adjusted to the same concentration and qRT-PCR was performed for 10 TMKs (TMK6, 56, 19, 60, 39, 63, 40, 65, 42 and 71) as previously described (Beck et al., 2005). See Supplementary Table S1 for primer sequences and annealing temperatures. The TMK threshold cycles (CTs) for 1C and 2C were then compared. As shown in Supplementary Fig. S1, 1C and 2C yielded similar CT values for all TMKs examined, indicating that the linearity of amplification was maintained throughout the second cycle.

For microarray validation, cDNA was prepared from a single cell as described above. The 2× amplified cDNA was diluted 1:100 with H_2O and qRT-PCR was carried out using iQSYBRGreen super mix (Bio-Rad, Hercules, CA, USA) and previously developed methods (Beck et al., 2005). Supplementary Table S1 lists primer sequences and annealing temperatures. Two "present" and two "absent" transcripts were selected for validation, and as a positive control cDNA was prepared from 10^6 trophozoites.

2.5. Antibodies

Peptides corresponding to amino acids (aa) 491–506 of TMK39 and 242–254 of TMK54 were synthesised, conjugated to Keyhole Limpet Haemocyanin and used to immunize New Zealand White rabbits. This work was contracted to Covance Research Products Inc., formal animal ethics approval was obtained and animal treatment was in accordance with all applicable laws and regulations. The resultant serum was affinity purified using immobilized peptide and dialysed against PBS. Resulting anti-TMK39 and anti-TMK54 antibodies were stored at −80 °C until use. Antibodies against TMK-96 (PaTMK) and the heavy subunit of the Gal/GalNAc lectin (Hgl) have been previously described (Petri et al., 1989; Boettner et al., 2008). Negative control, anti-Ft, an antibody which is directed against a *Francisella tularensis* protein, was a kind gift from Nicole Ark and Barbara Mann at the University of Virginia, USA. Polyclonal anti-actin (Santa Cruz Biotechnology, Santa Cruz, CA) and monoclonal anti-V5 (Sigma) antibodies were commercially available. For Western blotting, polyclonal antibodies were used at a concentration of 5 μg/ml, whereas monoclonal anti-V5 was used at 1 μg/ml. For confocal microscopy and flow cytometry antibody concentrations were doubled.

2.6. SDS–PAGE gels and Western blotting

Harvested trophozoites (HM-1:IMSS or induced HM-1:IMSS transfectants) were washed in PBS and lysed at a concentration of 10^4 amoebae/μL (50 mM Tris–HCl, pH 8.0, 150 mM NaCl, 1% Nonidet P-40, protease inhibitor cocktail (Sigma, St. Louis, MO, USA) and 0.02 mM E-64 (Sigma, St. Louis, MO, USA)). Cell lysate, immunoprecipitation or fractionated cellular sub-fractions (below) were resolved in 10% SDS–PAGE gels, transferred to polyvinylidene fluoride membrane using standard methods and membranes were blocked with 5% non-fat dry milk in Tris-buffered saline containing 0.1% (v/v) Tween-20 (TTBS) for 1 h at room temperature (RT). If noted, the membrane was cut into strips or primary antibodies (5 μg/ml) were pre-incubated with the indicated amount of unconjugated peptide for 1 h at RT prior to use. Primary antibodies diluted in TTBS were incubated with blocked membranes for 1 h at RT, membranes were washed with TTBS (5 × 5 min) and exposed to secondary antibody (anti-rabbit:AP or anti-mouse:AP) at a concentration recommended by the manufacturer (Sigma, St. Louis, MO, USA) for 1 h at RT. Finally, membranes were washed five times in TTBS and bands were visualised on film using the enhanced chemiluminescent (ECL) kit (Roche, Indianapolis, IN, USA).

2.7. Flow cytometry

Late-log phase *E. histolytica* trophozoites were harvested, washed twice with PBS and fixed with 3.7% paraformaldehyde (PFA) in PBS for 30 min at RT. If indicated, cells were permeabilized for 1 min with 0.2% Triton X-100 (Sigma, St. Louis, MO, USA) in PBS and non-specific binding was blocked by incubation with 20% goat serum and 5% BSA for 1 h at 37 °C. To assess TMK levels, permeabilized HM-1:IMSS trophozoites were stained for 1 h at 37 °C with anti-TMK39, anti-TMK54, anti-PaTMK (TMK-96), anti-Hgl (as a positive control) or anti-Ft (as a negative control).

To assess lectin levels, both non-permeabilized (cell surface Hgl) and permeabilized (total Hgl) transfected trophozoites were stained with anti-Hgl for 1 h at 37 °C. In both instances, Cy™ 3-conjugated Goat Anti-Rabbit IgG (Jackson Immuno Research, West Grove, PA, USA) was used as the secondary antibody at a 1:200 dilution in blocking buffer. As a control, cells were stained with secondary antibody only (no primary antibody). After 1 h incubation at 37 °C with the secondary antibody, samples were washed three times in PBS, re-suspended in 200 μl of PBS and analysed using a FACSCalibur (BD Biosciences) on channel FL2. In all instances, an intact amoeba gate was set prior to data collection (using side scatter (SSC) and forward scatter (FSC) and 10,000 gated events were collected for each sample. FlowJo software (http://www.treestar.com/flowjo/) was used for data analysis. All experiments were carried out three times or more and representative overlaid FL2 histograms are shown.

2.8. Fractionation

Cellular fractionation was carried out as previously described (Aley et al., 1980). Briefly, 10^8 trophozoites were harvested, washed twice with 19 mM potassium phosphate buffer, pH 7.2, and 0.27 M NaCl (PD). Cells were re-suspended to 2×10^7 amoebae/ml in PD + 10 mM $MgCl_2$ and mixed with an equal volume of 1 mg/ml concanavalin A in the same buffer. After 5 min at RT, cells were centrifuged at 50*g* for 1 min and the supernatant (containing excess conA) was discarded. The pellet was re-suspended in 12 ml of a hypotonic buffer containing 10 mM Tris–HCl, pH 7.5, 2 mM PMSF (Tris buffer) and 1 mM $MgCl_2$. After a 10 min swell, the cells were homogenised using 18–20 strokes of a glass Dounce homogenizer. A two-step gradient consisting of 0.5 M mannitol (8 ml) over 0.58 M sucrose (4 ml), both in Tris buffer, was prepared (gradient 1). The homogenate was layered on top and then centrifuged at 250*g* for 30 min. Large plasma membrane fragments formed a pellet at the bottom of gradient 1. The material remaining above gradient 1 was spun at 40,000*g* for 1 h to separate soluble cytoplasmic components (supernatant) from internal membranes (pellet). The plasma membrane pellet from the bottom of gradient 1 was re-suspended in 1 ml of Tris buffer + 1 M α-methyl mannoside and iced for 40 min with occasional mixing. The mixture was diluted into 3 volume of Tris buffer and homogenised with 80 strokes of a Dounce homogenizer. The homogenate was layered onto 20% sucrose in Tris buffer (gradient 2) and centrifuged at 250*g* for 30 min. Vesiculated plasma membranes that remained above gradient 2 were collected and concentrated by centrifugation at 40,000*g* for 1 h. The resulting pellet was re-suspended in Tris buffer and served as the plasma membrane fraction.

The three fractions used for analysis (soluble, internal membranes, and plasma membranes) were adjusted to equal volumes and analysed by Western blotting. As TMK39 and Hgl are similar in size (respectively, 127 kDa and 170 kDa), membrane panels

Please cite this article in press as: Buss, S.N., et al. Members of the *Entamoeba histolytica* transmembrane kinase family play non-redundant roles in growth and phagocytosis. Int. J. Parasitol. (2010), doi:10.1016/j.ijpara.2009.12.007

were first probed with anti-TMK antibodies and developed, then stripped with ReBlot Plus Strong Antibody Stripping solution (Millipore, Billerica, MA, USA) and re-probed with anti-Hgl antibodies.

2.9. Confocal microscopy

E. histolytica trophozoites (HM-1:IMSS) in TYI-S-33 medium were allowed to adhere to glass coverslips in a 24-well plate for 1 h at 37 °C at a concentration of 5.0×10^5 trophozoites/well. Adherent amoebae were washed with warm PBS and fixed with 3.7% PFA for 30 min at RT. Non-specific binding was blocked with 20% goat serum and 5% BSA (Sigma, St. Louis, MO, USA) in PBS (1 h at 37 °C). Cells were stained for 1 h at 37 °C with anti-TMK antibodies diluted in blocking buffer. If indicated, primary antibodies were pre-incubated with 300 nM unconjugated peptide for 1 h at RT. Cells were then washed three times with PBS and Cy3-conjugated goat anti-rabbit secondary antibodies (Jackson Laboratories, Bar Harbor, ME, USA) were added at a 1:200 dilution (in blocking buffer) for 1 h at 37 °C. After three washes, coverslips were mounted to slides with Fluoromount-G (Southern BioTech, Birmingham, AL, USA). A Zeiss LSM 510 laser-scanning microscope was used to visualise cells and final images were analysed using LSM Image Browser software (Carl Zeiss, Inc., Thornwood, NY, USA).

2.10. Inducible expression vectors

For expression of truncated proteins containing V5 and 6× His tags, the indicated regions of TMK39 and TMK54 were PCR amplified with the primers: 39F -CACC ATG TTT CTT TTA TTT ACA ATC CTC, 39R -AAT AAT AAT AAG AAT AAT CAC AAT CAG, 54F -CACC ATG TTG CTT CTT TTT TCA CTT ATT TCA, 54R -ACC AAG AAA TAT TAA AAT AGA TAA TAT AG. These fragments were cloned into the Gateway pENTR™/SD/D-TOPO® (Invitrogen) plasmid, sequence verified and Gateway® LR Clonase™ II Enzyme Mix (Invitrogen) was used, according to manufacturer's instructions, to transfer the truncated TMK fragments into the Gateway® pET-DEST42 vector in-frame with the C-terminal epitope tags. Truncated TMK fragments and tags were then PCR amplified from the pET-DEST42 vector with N-terminal *Kpn*I and C-terminal *Bam*HI restriction sites using the primers: K39F -CTA CTG GGT ACC ATG TTT CTT TTA TTT ACA ATC CTC, K54F -CTA CTG GGT ACC ATG TTG CTT CTT TTT TCA CTT ATT TCA, *Bam*HisR -ATA ATG GGA TCC TCA ATG GTG ATG GTG ATG ATG. Resulting PCR products were cloned into the *Kpn*I and *Bam*HI sites of the digested and gel purified pEhHYG-tetR-O-CAT vector (Hamann et al., 1997). Final constructs were sequence verified and the parental pEhHYG-tetR-O-CAT vector was used as a control.

2.11. Transfection of E. histolytica trophozoites

The GenElute™ HP Plasmid Maxiprep Kit (Sigma, St. Louis, MO, USA) was used to prepare plasmid DNA and DNA was quantified using the NanoDrop™ 2000 (Thermo Fisher, Wilmington, DE, USA). A known quantity of DNA was precipitated using standard methods and re-suspended to a concentration of 200 μg/ml in supplemented (5.7 mM cysteine, 25 mM HEPES and 0.6 mM ascorbic acid) and filter-sterilized Medium 199 (M199S) (Invitrogen, Carlsbad, CA, USA), that had been adjusted to pH 7.0. One hundred microlitre of the DNA (20 μg) was mixed with 15 μl of Attractene or SuperFect (Qiagen, Valencia, CA, USA) and incubated as per the manufacturer's instructions to allow formation of transfection complexes. Log-phase trophozoites were then harvested on ice, washed in M199S and re-suspended to a concentration of 5.0×10^5 amoebae/ml in M199S supplemented with 15% heat-inactivated bovine serum. Processed amoebae (0.9 ml) were added to transfection complexes and incubated for 3 h at 37 °C. After the incubation period, amoebae were added to 25 cm^2 tissue culture flasks containing complete TYI-S-33 medium supplemented with 100 U/ml of penicillin and 100 μg/ml streptomycin (Invitrogen, Carlsbad, CA, USA). After 18 h at 37 °C, transfected cells were selected using 15 μg/ml hygromycin (Invitrogen, Carlsbad, CA, USA). Debris from dead cells was removed and fresh media added beginning 4–5 days post-selection. Approximately 2 weeks after selection, transfectants obtained log-phase growth. Following 24 h of induction with 10 μg/ml of tetracycline, expression was verified by Western blotting using a monoclonal anti-V5 antibody (Sigma) as described.

2.12. Immunoprecipitation

Transfected cells were induced for 24 h and lysed on ice at a concentration of 10^7 amoebae/ml in 50 mM Tris–HCl, pH 8.0, 150 mM NaCl, 1% Nonidet P-40, protease inhibitor cocktail (Sigma, St. Louis, MO, USA) and 0.02 mM E-64 (Sigma). Cellular debris was removed by centrifugation at 9500*g* for 10 min at 4 °C. V5-agarose was washed in PBS five times and 20 μl of the washed agarose was added to 100 μl of cleared lysate. The mixture was incubated for 1.5 h at 4 °C on a shaker. Following the incubation period, the resin was washed three times in lysis buffer diluted 1:1 with PBS and twice in PBS. Twenty microlitre PBS and 5 μl 5× SDS–PAGE sample buffer were added to the agarose; the samples were heated to 95 °C for 10 min and analysed via Western blot.

2.13. Growth curves

Transfected (parental vector, t-39 or t-54) and non-transfected HM-1:IMSS trophozoites were harvested during log-phase growth and 10,000 cells were seeded into 15 ml of TYI-S-33 media that contained 10 μg/ml of tetracycline. Parasite numbers were recorded every 24 h for 4 days and expression of the protein was verified each day, in parallel. At least two independently transfected clones were tested, each sample was assayed in triplicate and results represent the mean of three or more experiments.

2.14. Amnis Imagestream data collection and analysis

Phagocytosis assays were carried out as described below, using 2×10^6 *E. histolytica* trophozoites and 2×10^7 carboxylate-modified 2.0 μm fluorescent yellow-green beads (Sigma, St. Louis, MO, USA). Following PFA fixation, amoebae were permeabilized with 0.2% Triton X-100 in PBS for 1 min if indicated and paraformaldehyde was neutralised with 50 mM NH_4Cl. Non-specific binding was then blocked by incubation (1 h at 37 °C) with 10% goat serum in PBS (blocking buffer). TMKs were detected by incubation for 1 h at 37 °C with anti-TMK antibodies diluted to 15 μg/ml in blocking buffer. Three PBS washes were performed and R-PE-conjugated goat anti-rabbit secondary antibodies (Jackson Laboratories, Bar Harbor, ME, USA) were added at a 1:200 dilution for 1 h at 37 °C. Following the incubation, samples were washed with PBS three times, re-suspended in 50 μl PBS and filtered through a 70 μm nylon cell strainer (BD Falcon, Bedford, MA, USA). Where indicated the procedure was carried out in the absence of amoebae (stained beads) or in the absence of anti-TMK antibodies (secondary only). At least 5000 images were collected using the Amnis Imagestream imaging cytometer (Amnis Corporation; Seattle, WA, USA) and ImageStream Data Exploration and Analysis Software (IDEAS) was used for data analysis. Prior to data analysis, spectral compensation was performed using "stained" beads and stained cells. Raw image files from the same experiment were all compensated with the same matrix and all compensated image files from the same experiment were opened with the same template. In each

Please cite this article in press as: Buss, S.N., et al. Members of the *Entamoeba histolytica* transmembrane kinase family play non-redundant roles in growth and phagocytosis. Int. J. Parasitol. (2010), doi:10.1016/j.ijpara.2009.12.007

template, gating was performed to generate a population of single, in-focus, bead-positive cell images (usually yielding 500–1000 images per sample) and masking was used to identify beads and the brightest 20% of antibody staining. Within the template, the Bright Detail Similarity (BDS) feature was used to calculate the extent of correlation between the two masks and thus quantify the extent of co-localisation between ingested beads and TMKs. BDS scores $\geqslant 3$ are considered co-localised.

2.15. Fluorescent labelling and killing of cells

Ficoll-Paque™ Plus (GE Healthcare, UK) isolated Jurkat cells or packed erythrocytes were suspended in 0.1% BSA in PBS at a concentration of 5×10^6/ml and incubated with 5 μM carboxyfluorescein succinimidyl ester (CFSE) for 10 min at 37 °C. FBS was used to quench unbound dye and the cells were washed three times with RPMI media. Jurkat cells were then killed using UV irradiation, whereas erythrocytes were calcium-treated by incubation at 37 °C for 48 h in HEPES buffer containing 2.5 mM $CaCl_2$. Both methods have been described elsewhere (Bratosin et al., 2001; Teixeira and Huston, 2008).

2.16. Phagocytosis assays

Phagocytosis was assayed by flow cytometry as previously described (Huston et al., 2003). Particles used for ingestion assays included fluorescent green 2.0 μm carboxylate-modified latex beads (Sigma, St. Louis, MO, USA), CFSE-labelled apoptotic Jurkat cells and Ca^{2+} treated red blood cells. Amoebae were induced with 10 μg/ml of tetracycline for 24 h. Particles were then mixed with amoebae at a 5:1 ratio, centrifuged for 5 min at 200g and incubated at 37 °C for 30 min. D-Galactose (110 mM) in ice-cold PBS was used to wash away non-ingested material and cells were fixed with 3.7% PFA. Samples were washed, re-suspended in PBS and analysed using a FACSCalibur (BD Biosciences) on channel FL1. SSC and FSC were used to distinguish amoebae from non-ingested particles and a live cell gate was established prior to data collection with 10,000 gated events collected for each sample. The mean fluorescence intensity (MFI) was calculated for each sample, background fluorescence was subtracted and data was plotted as a percentage of control MFI. Cell types were assayed in duplicate (at minimum) and the experiments were repeated at least three times. Data represents the mean of all experiments and error bars represent the SD.

2.17. Pinocytosis assay

Pinocytosis was assayed in a similar manner to phagocytosis, however 1 mg/ml FITC-dextran (Sigma) in PBS was incubated with amoebae instead of a particle. Incubation times and procedures were otherwise the same.

3. Results

3.1. Single cell TMK gene expression analysis

LCM was used in conjunction with microarray analysis to examine TMK gene expression at the single cell level. RNA isolated from a laser-captured *E. histolytica* trophozoite was subjected to two cycles of amplification and analysed via microarray (Supplementary Fig. S1). Affymetrix® GCOS was then used to generate detection calls for each TMK probe set. Multiple TMK transcripts were detected as present within a single cell (Table 1). The experiment was carried out in duplicate and TMK transcripts identified within both cells are underlined in Table 1. Average log intensity values for TMKs and reference genes are listed in Supplementary Table S2. Multiple TMK genes were expressed in both cells, and one cell expressed detectable levels of multiple members of TMK sub-groups A, B_1, D_1 and E. Microarray results were validated by qRT-PCR conducted on RNA isolated from an independently laser-captured trophozoite (data not shown). The presence of multiple TMK transcripts within a single cell indicated that these genes do not undergo antigenic variation at the level of transcription.

3.2. Protein expression analysis

To enable examination of TMK expression at the protein level, polyclonal antibodies directed against unique peptides within the extracellular domains of TMK39 (sub-family C) and TMK54 (sub-family E) were generated. Peptides were chosen for immunization by first manually identifying hydrophilic and cysteine-free stretches of sequence in each extracellular domain and then using the Basic Local Alignment Search Tool (BLAST) to check the sequences against the *E. histolytica* Genome Project Database and ensure specificity. Resultant antibodies were deemed specific as both recognised single bands of the predicted size in *E. histolytica* lysate and both bands disappeared when the antibodies were pre-incubated with increasing amounts of the corresponding unconjugated peptide (Fig. 1A). An anti-peptide antibody against PaTMK (TMK-96, sub-family B_3) has previously been developed and was also used in the following studies (Boettner et al., 2008).

Expression of PaTMK and sub-family B_1 TMKs has been examined at the protein level (Mehra et al., 2006; Boettner et al., 2008) however studies have been limited to Western blotting and microscopy. Consequently, it is unknown whether TMKs are heterogeneously expressed by trophozoites within a population. To examine expression of TMKs at the population level, we labelled permeabilized trophozoites with anti-TMK39, anti-TMK54 or anti-PaTMK, and analysed the samples by flow cytometry. In these experiments, trophozoites were harvested from the same flask, immediately fixed with 3.7% PFA and then stained. Flow cytometric

Table 1
Transmembrane kinase (TMK) transcripts detected in a single, *Entamoeba histolytica* trophozoite. Single cells expressed more than one TMK. RNA from a single amoeba isolated by laser-capture microdissection (LCM) was purified using the PicoPure™ RNA Isolation Kit and subjected to two cycles of amplification using the WT-Ovation™ Pico System. Resulting cDNA was hybridized to the E_his-1a520285 custom array (Affymetrix). The arrays were then stained using the standard Affymetrix protocol for eukaryotic targets. An Affymetrix Gene Chip scanner 3000 I was used to scan the arrays and report files were generated to determine the percentage of present calls. The experiment was carried out twice. TMK transcripts identified are listed, with those identified in both amoebae underlined. Validation of microarray results was carried out by quantitative reverse transcription PCR (qRT-PCR) (data not shown). cDNA samples used for microarray analysis and qRT-PCR validation were generated from different amoebae. For the validation, RNA was purified from a single cell and amplified (two rounds) as described. The mRNA abundance of two GCOS "present" (XM648585 and XM648643) and two GCOS "absent" (XM643895 and XM650501) transcripts was then measured by qRT-PCR. There was agreement in every instance.

TMK group	TMK#	GenBank XM#
A	TMK17	XM646584
	TMK23	XM647001
	TMK65	XM649022
B_1	TMK14	XM646638
	TMK87	XM644636
B_3	TMK35	XM645723
D_1	TMK03	XM646909
	TMK40	XM648928
D_2	TMK19	XM646939
E	TMK22	XM651330
	TMK54	XM648585
F	TMK06	XM644657
	TMK59	XM644333

Please cite this article in press as: Buss, S.N., et al. Members of the *Entamoeba histolytica* transmembrane kinase family play non-redundant roles in growth and phagocytosis. Int. J. Parasitol. (2010), doi:10.1016/j.ijpara.2009.12.007